Physics – Uspekhi **65** (3) 245 – 269 (2022)

REVIEWS OF TOPICAL PROBLEMS PACS numbers: **42.50. – p**, **42.79. – e**, **78.67. – n**

Quantum optics of quantum emitters in the near field of a nanoparticle

Yu V Vladimirova, V N Zadkov

DOI: https://doi.org/10.3367/UFNe.2021.02.038944

Contents

Abstract. This review is devoted to studies of quantum optics effects for quantum emitters (QEs) in the near field of nanoparticles (NPs). In the simple model of a two-level QE located near a plasmon NP, we analyze the mechanisms for modifying the radiative and nonradiative decay rates and discuss the distribution of the near-field intensity and polarization around the NP. This distribution has a complex structure, being significantly dependent on the polarization of the external radiation field and on the parameters of NP plasmon resonances. The quantum optics effects in the system (NP + QE + external laser field) are analyzed, including the near-field modification of the resonance fluorescence spectrum of a QE, the bunching/antibunching effects and photon quantum statistics effects in the spectrum, the formation of squeezed light states, and quantum entangled states in such systems.

Keywords: nanophotonics, nanoplasmonics, nanostructure, quantum emitter, two-level system, quantum optics, resonance fluorescence, antibunching and quantum statistics of photons, squeezed states, quantum entangled states

Yu V Vladimirova [(1, 2, a)], **V N Zadkov** [(2, 3, b)]
[(1)] Lomonosov Moscow State University, Department of Physics, Quantum Technology Center,
Leninskie gory 1, str. 35, 119991 Moscow, Russian Federation
[(2)] National Research University Higher School of Economics, Department of Physics, ul. Staraya Basmannaya 21/4, str. 5, 105066 Moscow, Russian Federation
[(3)] Institute of Spectroscopy, Russian Academy of Sciences, ul. Fizicheskaya 5, 108840 Troitsk, Moscow, Russian Federation
E-mail: [(a)]yu.vladimirova@physics.msu.ru, [(b)]zadkov@isan.troitsk.ru

Received 19 August 2020, revised 13 January 2021
Uspekhi Fizicheskikh Nauk **192** (3) 267 – 293 (2022)
Translated by S Alekseev

1. Introduction

In this review, we discuss the effects of quantum optics of single quantum emitters (QEs) (atoms, molecules, quantum dots, NV centers, etc.) in the near field of a nanoparticle (NP). The range of problems to be discussed has to be defined, because the term 'quantum plasmonics,' which has been widely used recently in the scientific literature, refers to a new area of studies in nanophotonics: a combination of nanoplasmonics and quantum optics [1]. This includes interactions of QEs not only with the plasmons localized inside an NP but also with surface plasmon waves, when their quantum properties also play a significant role. We first consider effects such as the nonclassical behavior of light in the resonance fluorescence of a single atom [2], manifested as the sub-Poisson distribution of the photon statistics [3], the antibunching of scattered photons [4] in the count of delayed coincidences, as well as the nonclassical behavior of light in the distribution of photocounts and in the spectrum of intensity fluctuations.

These and other quantum effects arising in QE + NP + external field systems are of special current interest due to the rapid development of experimental studies in the field of nanophotonics, which, in particular, provides reliable sources of nonclassical light from single QEs, including those embedded in various nanostructures [5]. We primarily consider and use the following unique properties of NPs and nanostructures (Fig. 1):

(1) Effective conversion of the electromagnetic radiation interacting with an NP to the near electromagnetic field, which ensures a multiple increase in the field intensity in the subwavelength range around the NP [6–8].

(2) The control of the spontaneous emission parameters of a QE in the near field of the NP (the Purcell effect) [9].

(3) The ability to concentrate and redirect the incident radiation into a specified spatial domain, i.e., control of the radiation pattern [10].

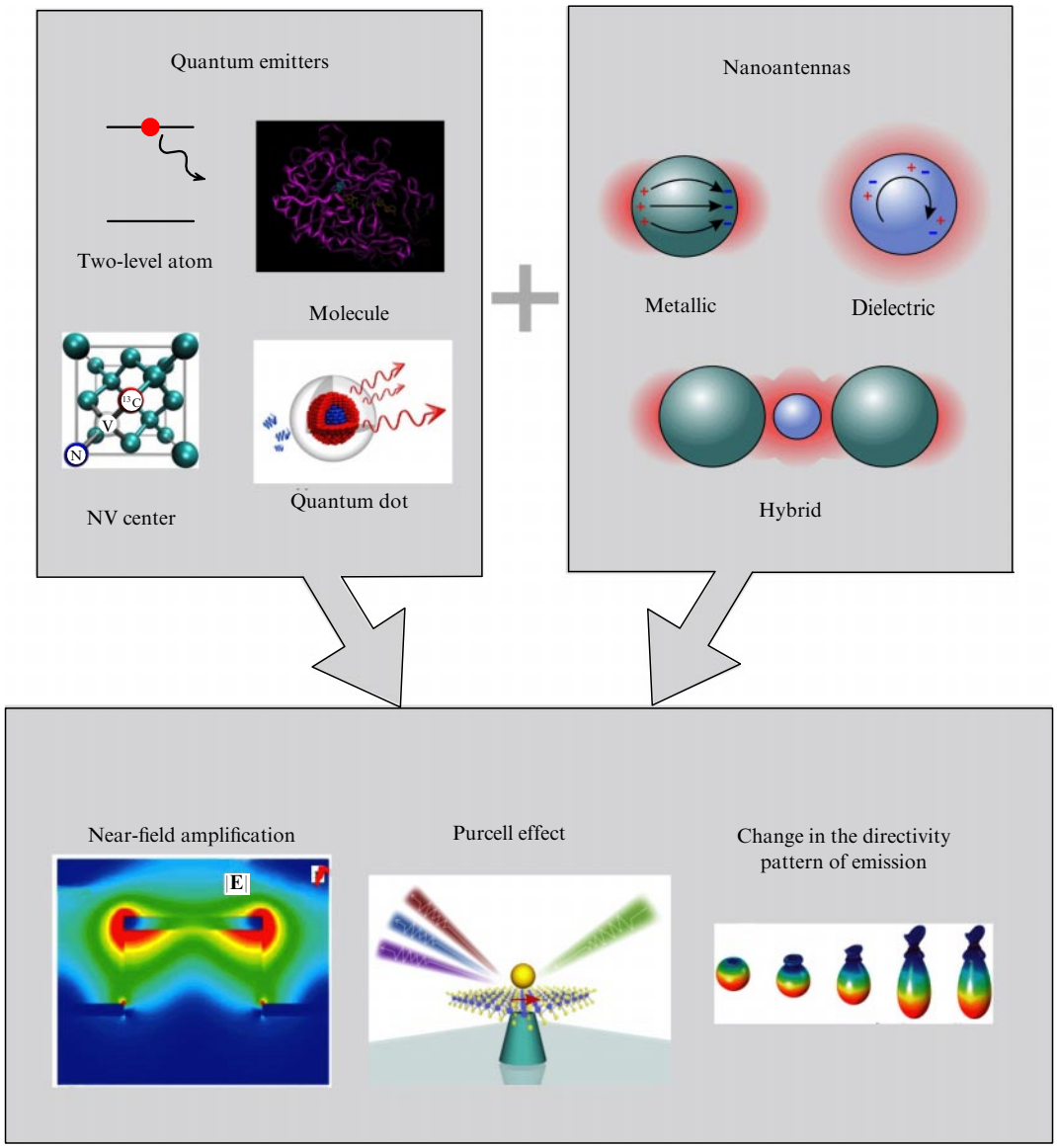

Figure 1. (Color online.) Properties of nanoantennas as regards controlling an electromagnetic field on the nanoscale and changing spontaneous QE emission parameters in the near field of a nanoantenna.

Nanostructures with such properties, often referred to as *optical nanoantennas*, have great potential in various areas of research: in the tasks of optical processing of information [11–13], in producing single-photon sources [14], in photovoltaics [15–19], in medicine for therapy of oncological diseases [20–24], in super-resolution microscopy problems [25, 26], and in many others. Numerous reviews and books are devoted to optical antennas [5, 27–35], and here we only briefly focus on the basic properties of such antennas, as long as they are important in describing the interaction of QEs with NPs.

Optical nanoantennas can be divided into three groups: metal, dielectric, and hybrid (metal–dielectric). Each group has its advantages and disadvantages.

Metal nanoantennas, called plasmonic nanoantennas, allow localizing the excitation electromagnetic field on a scale of about 10 nm in the near zone due to the excitation of plasmon resonance in them. Traditionally, such antennas are made of chemically resistant noble metals, such as gold or silver, whose dissipative losses in the visible range, even if the lowest among metals, are still rather high [36, 37]. Of importance is not only the material from which the nanoantenna is made but also its geometry, which significantly affects the near-field amplification and the Purcell factor. For example, it was shown in [38] that a solution with gold nanospheres 35 nm in diameter does not produce fluorescence, but a solution with gold nanorods of the same volume leads to an increase in fluorescence by 6 to 7 orders of magnitude. The ability of metal nanoantennas to amplify the near field by several orders of magnitude plays an important role in thermoplasmonics and medicine [39], but their use in systems requiring effective transmission of the electromagnetic energy is obviously ineffective.

The limitations specific to metal nanoantennas are overcome by *dielectric nanoantennas*, which are manufactured from materials (for example, Si) with a high refractive index and low absorption coefficient in the visible range [40]. Both electric and magnetic resonances are excited inside the dielectric nanostructure [41–43], allowing nanoantennas to interact with the electric and magnetic components of the electromagnetic field equally, whereas plasmonic antennas

interact only with the electric component. However, the amplification of the near field of dielectric antennas is noticeably weaker than that of plasmonic ones, resulting in a lower Purcell factor.

The above advantages and disadvantages of metallic and dielectric nanoantennas motivated the creation of so-called *hybrid nanoantennas*, which combine the advantages of metallic and dielectric ones [29]. The development of such nanostructures has been actively carried out recently. Studies show that hybrid nanoantennas have many interesting properties in terms of practical use, including low heat losses, optical and magnetic resonance responses, pronounced nonlinear-optics features, and the ability to control the radiation pattern.

The presence of nanoantennas of any type near a QE affects its properties (radiation intensity, quantum throughput, spectrum of resonance fluorescence, and photon statistics from the spectrum of resonance fluorescence) and also leads to antibunching of photons and radiation squeezing, generating quantum entangled states. All the properties just mentioned depend on the electromagnetic field strength and polarization, the spontaneous relaxation rate, and the QE transition frequency [44].

In Section 2, we consider theoretical approaches to the study of the distribution of the near field strength and polarization of a plasmonic NP.

In Section 3, we describe the effects of the interaction of a single QE with a nanoantenna within the classical and quantum approaches, the options for controlling QE parameters by changing NP parameters, and QE fluorescence quenching near a nanoantenna. We also discuss different types of nanoantennas, paying some extra attention to promising hybrid nanoantennas.

Section 4 is devoted to the effects of single-QE quantum optics in the near field of an NP placed in an external electromagnetic field. We discuss the generation of the spectrum of the QE resonance fluorescence, the photon antibunching phenomenon, the formation of compressed states of light, the sub-Poissonian statistics of photon counts from the resonance fluorescence spectrum, and the generation of quantum entangled states.

In Section 5, we summarize the effects of quantum optics of a single QE in the near field of an NP and discuss their applications.

2. Near field of a nanoparticle in an external electromagnetic field. Polarization of the nanoparticle near field

The simplest geometric shape of an NP is a sphere. We begin our discussion with such NPs especially, because an analytic solution to the corresponding diffraction problem is available for the spherical geometry (it was first obtained by Mie [41] in 1908). Mie's theory applied to spherical NPs is considered in detail in the literature [29, 34, 45]. In [45], the problem of plane wave scattering on a spherical particle was considered in detail; the focus in [34] was on the excitation of spherical particles of point-like QEs (atoms, molecules, quantum dots, or NV centers). The problem of a QE placed inside a spherical NP into which, for example, fluorophore molecules are introduced was also solved in [46].

Further development of Mie's theory has allowed the optical properties of spheroidal-geometry NPs (nanorods, nanoneedles, nanodiscs) to be calculated analytically. These problems are already much more complicated, because they require the calculation of spheroidal functions, for which effective algorithms were purposely developed [47, 48]. In the case of complicated geometries, the only way to solve the problem is by solving the Maxwell equations numerically; a number of effective numerical methods have been developed for this.

Directly solving the Maxwell equations is not always the optimal strategy, however. For example, a numerical solution of the Maxwell equations for scattering of the electromagnetic field of an NP made of one material cannot be directly used to determine the plasmonic properties of an NP of the same shape but made of another material. Finding exact values of plasmon frequencies and other characteristics of plasmons with this solution method is a challenge. It is convenient to use the so-called ε-method instead, where the main role is played not by resonance frequencies but by the corresponding dielectric permittivity values.

This method, developed in [49, 50], allows finding the near field of an NP from its plasmon spectrum, i.e., the eigenfunctions $\mathbf{e}_n$ and $\mathbf{h}_n$ satisfying the Maxwell equations

$$\begin{aligned} &\operatorname{rot}\mathbf{h}_n + \mathrm{i}k\varepsilon_n\mathbf{e}_n = 0\,, \\ &\operatorname{rot}\mathbf{e}_n - \mathrm{i}k\mathbf{h}_n = 0\,, \end{aligned} \tag{1}$$

and the continuity conditions for the tangential components on the NP surface together with Sommerfeld's radiation conditions. The electric field near the NP of an arbitrary shape is given by

$$\mathbf{E}(\mathbf{r},\omega) = \mathbf{E}_0(\mathbf{r}) + \sum_n \mathbf{e}_n \frac{\varepsilon(\omega)-\varepsilon_{\mathrm{env}}}{\varepsilon_n-\varepsilon(\omega)} \frac{\int_V (\mathbf{e}_n,\mathbf{E}_0)\,\mathrm{d}V}{\int_V \mathbf{e}_n^2\,\mathrm{d}V}\,, \tag{2}$$

where $\varepsilon(\omega)$ describes the frequency dependence of the dielectric permittivity of a particular material from which the NP is made, $\mathbf{e}_n$ and ε_n are the plasmon oscillation mode and its eigenvalue, $\varepsilon_{\mathrm{env}}$ is the dielectric permittivity of the environment, $\mathbf{E}_0$ is the field in the absence of an NP, and V is the NP volume. $\mathbf{H}(\mathbf{r},\omega)$ is defined in the same way modulo the replacement $\mathbf{e}_n \to \mathbf{h}_n$, $\mathbf{E}_0 \to \mathbf{H}_0$. Expression (2) is exact and describes an NP of any size, because the delay effect is entirely taken into account there.

The problems covered in this review include optical fields in the visible range, i.e., in the case where the wavelength of the external field is much greater than the linear particle size, $\lambda \gg l$. Then, the quasistatic approximation can well be used to determine the near fields $\mathbf{e}_n$. In this case, the field near the NP, according to (2), is given by

$$\mathbf{E} = \mathbf{E}_0 + \sum_n \frac{\varepsilon(\omega)-\varepsilon_{\mathrm{env}}}{\varepsilon_n-\varepsilon(\omega)} \frac{\int_V (-\nabla\varphi_n,\mathbf{E}_0)\,\mathrm{d}V}{\int_V (\nabla\varphi_n)^2\,\mathrm{d}V}(-\nabla\varphi_n)\,, \tag{3}$$

where φ_n are the potentials of the corresponding plasmon modes $\mathbf{e}_n$.

Polarization of the near field of a nanoparticle. When speaking of the near field in the context of nano-optics and nanoplasmonics, only its strength is usually interesting, because it can be measured experimentally. But an equally important characteristic of the field is its polarization, and the interaction of a QE with the field is substantially dependent on the polarization of the latter.

In [51, 52], the polarization of the near field of metallic and dielectric NPs of spherical and spheroidal geometries was studied in detail. Following these papers, we consider the

polarization of the near field of a plasmonic NP. Let the field at a point **r** be

$$E_x(\mathbf{r},t) = A_x(\mathbf{r})\cos\left[\omega t + \phi_x(\mathbf{r})\right],$$
$$E_y(\mathbf{r},t) = A_y(\mathbf{r})\cos\left[\omega t + \phi_y(\mathbf{r})\right], \quad (4)$$
$$E_z(\mathbf{r},t) = A_z(\mathbf{r})\cos\left[\omega t + \phi_z(\mathbf{r})\right],$$

where $A_i(\mathbf{r})$ (with $i = x, y, z$) is the actual amplitude of the ith component of the near field **E** in formula (3) and $\phi_x(\mathbf{r})$, $\phi_y(\mathbf{r})$, and $\phi_z(\mathbf{r})$ are the phases of field projections on the coordinate axes. By eliminating the time dependence, it can be shown that the curve described by the vector **E** over the field oscillation period lies in the plane whose orientation is determined by the amplitudes A_i and the phase shifts ϕ_x, ϕ_y, and ϕ_z. Because all components of **E** change with the same frequency, the vector **E** describes oscillations of an ellipse whose semiaxes are equal to the minimum, $E_{\min}$, and the maximum, $E_{\max}$, values of the field amplitude at the chosen spatial point. If the minimum value of the field amplitude is zero, then the polarization is linear, and if $E_{\min} = E_{\max}$, then it is circular.

To quantify the near-field polarization at each point, we introduce the degree of polarization

$$P = \frac{I_{\max} - I_{\min}}{I_{\max} + I_{\min}}, \quad (5)$$

where $I_{\max}$ and $I_{\min}$ are the maximum and minimum values of the modulus of the Poynting vector at this point over the period of the electromagnetic wave oscillations. This quantity shows how close the field polarization is to the linear one. We have $P = 1$ for the linear and $P = 0$ for the circular polarization; in the case of elliptical polarization, P takes values between 0 and 1.

The quantity P is fundamentally different from the degree of polarization that characterizes the polarization of the field and for a plane wave is defined as

$$\tilde{P} = \frac{\sqrt{S_1^2 + S_2^2 + S_3^2}}{I}, \quad (6)$$

where S_1, S_2, and S_3 are Stokes parameters. Having found $I_{\max}$ and $I_{\min}$ at a given point **r** in terms of the field components, we can easily calculate polarization degree (5). We note, however, that this does not provide complete information on the polarization of the near field, because polarization degree (5) does not specify the direction of rotation of the **E** vector. To determine the direction of rotation, it is convenient to use the Stokes parameters. But because the near field has three components in the general case, the so-called generalized Stokes parameters must be used to describe the state of polarization in this way [53]. In the three-dimensional case, the number of Stokes parameters is equal to nine. Three of them play a role similar to that of S_3 for each of the three planes xy, yz, and xz, and determine the predominance of the right circularly polarized field components over the left ones. These parameters can be expressed as

$$S_{3xy} = \mathrm{i}\left[\left\langle E_x^*(\mathbf{r},\omega)E_y(\mathbf{r},\omega)\right\rangle - \left\langle E_x(\mathbf{r},\omega)E_y^*(\mathbf{r},\omega)\right\rangle\right],$$
$$S_{3xz} = \mathrm{i}\left[\left\langle E_x^*(\mathbf{r},\omega)E_z(\mathbf{r},\omega)\right\rangle - \left\langle E_x(\mathbf{r},\omega)E_z^*(\mathbf{r},\omega)\right\rangle\right], \quad (7)$$
$$S_{3yz} = \mathrm{i}\left[\left\langle E_y^*(\mathbf{r},\omega)E_z(\mathbf{r},\omega)\right\rangle - \left\langle E_y(\mathbf{r},\omega)E_z^*(\mathbf{r},\omega)\right\rangle\right],$$

where $E_i = A_i \exp(\mathrm{i}\omega t)$ and the angular brackets denote averaging in time. In our case, the field is stationary, and therefore the averaging operation can be omitted. The parameter S_3 takes negative values if the left circular polarization is dominant, and positive values if the right one is dominant.

In terms of the three-dimensional Stokes parameter, the degree of polarization can be written as

$$P = \sqrt{1 - \left(\frac{S_{3xy}}{I}\right)^2 - \left(\frac{S_{3xz}}{I}\right)^2 - \left(\frac{S_{3yz}}{I}\right)^2}, \quad (8)$$

where the Stokes parameters are for convenience normalized to the field strength at the observation point.

In [51], the polarization of the near field of a spheroidal silver NP excited by a plane wave with linear, circular, and elliptical polarizations was studied. In the case of an NP interacting with a plane electromagnetic wave, only dipole modes are excited in the NP.

If the external field is linearly polarized along the z-axis, then only one plasmon mode with $n = 1$, $m = 0$ is excited. Figure 2 shows the distribution of the degree of polarization of the near field in the case of plasmon resonance for different plane wave polarizations ($k \parallel z$): linear (Fig. 2a), elliptical (Fig. 2b), and left circular (Fig. 2c), and also for an NP interacting with a single-mode Gaussian beam (Fig. 2d). In the last case, higher-order plasmon modes are excited in the beam field, which significantly complicates the polarization pattern of the near field.

It follows that the degree of the polarization pattern is strongly dependent on the polarization of the external field and has a complex structure. Near the NP surface, there are regions where the polarization is opposite to that of the external field: in the case of a linearly polarized external field, the distribution of the degree of polarization is shaped like two symmetric tori, in the center of which polarization is circular; by contrast, when the external field polarization is circular, the distribution of the degree of polarization has a complex shape, although still with linear polarization in the center. For a linearly polarized external field, the areas where polarization changes are reduced and shift toward the nanoantenna tip for $\alpha < \alpha_{\mathrm{res}}$ or to the spheroid equator for $\alpha > \alpha_{\mathrm{res}}$, where α is the aspect ratio, equal to the ratio of a minor semiaxis of a spheroid to its major semiaxis. Importantly, the position of the regions can be controlled by changing the incident radiation direction.

In [54], the polarization of the near field in the same system was studied using the isotropy parameters L^{T} and C^{T}. These parameters characterize the distribution of ellipses near the singular points. A numerical algorithm that tracks the lines L^{T} and C^{T} allows visualizing the lines of polarization singularities near the nanospheroid.

We note that a large number of theoretical studies deal with NP properties in free space, although in real experiments NPs are surrounded by other objects, such as other NPs or the underlying substrates. In some cases, the influence of the environment can be neglected, but this is not always a legitimate simplification. The influence of the substrate can be quite significant, for example, when creating near-field sensors, as well as in the popular method of surface-enhanced Raman scattering [55].

In [56], the distribution of near field polarization in the vicinity of a silver nanospheroid located on a quartz substrate was investigated. As in the absence of a substrate, the near-

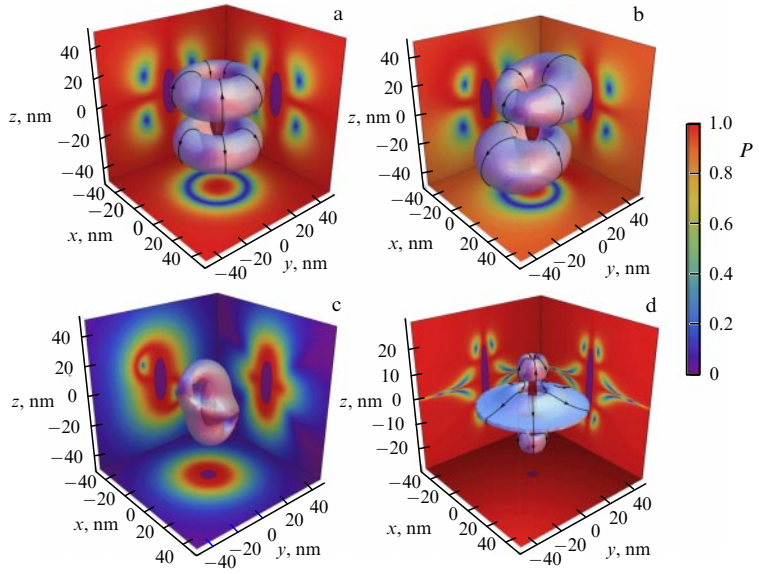

Figure 2. (Color online.) Distribution of the near-field polarization degree for plasmon resonance $\alpha = \alpha_{\text{res}}$. Three-dimensional surface corresponds to value $P = 0.8$. Two-dimensional distributions describe sections in the three planes: (a, b) xz and yz with $z = 15$ nm and (c, d) xy. Red color corresponds to the linear polarization ($P = 1$), magenta to the circular one ($P = 0$). Rotation direction of the E vector is shown by arrows.

field polarization is reversed near the spheroid surface. However, the distribution of the degree of polarization for an NP in free space is symmetric relative to both major and minor axes of the spheroid, but, in the presence of a substrate, the regions where polarization changes are only observed in the substrate for wavelengths near the plasmon resonance, and the size of these areas inside the substrate decreases. At the exact resonance, the size of the opposite-polarization region inside the substrate is roughly halved compared to the size of the area above the substrate. Far from the plasmon resonance, the opposite-polarization areas are absent in the substrate.

The near-field polarization has been studied for nanospheres made of a dielectric with a high refractive index (Si) both in free space and on a quartz substrate [57, 58]. In the case of a dielectric NP, the region where polarization changes is most pronounced at wavelengths that correspond to the electric and magnetic dipole and quadrupole resonances. As in the case of a metal NP, the regions of polarization reversal form near the NP surface, but the shape of these regions is different. In [59], the near-field polarization for a nanosphere made of a dielectric with a high refractive index (Si) was studied in free space using the isotropy parameters L^{T} and C^{T}.

3. Spontaneous emission of a quantum emitter in the presence of a nanoparticle

After the invention of the laser in 1960, quantum electronics underwent intensive development toward the use of controlled stimulated quantum processes to improve all characteristics of laser radiation. It was only 40 years later that, due to the development of nanotechnologies, the problem of controlling the elementary process of spontaneous emission by a QE (an atom, a molecule, or a quantum dot) started being actively addressed. Controlling this process underlies a wide range of applications, such as heterostructure-based LEDs [60], analytical chemistry, spectroscopy, and sensors [61].

A fluorescent QE interacting with the substance on a nanoscale is an ideal choice for a tag in various technologies, such as gene sequencing [62, 63], neural mapping [64], monitoring food and drug safety [65], and some others [66]. At the same time, spontaneous emission of a single QE in free space is too weak to be detectable in the case of low QE concentrations. In addition, because the radiation pattern of such a QE has no preferred direction, the problem of efficient signal detection arises. To overcome these disadvantages, methods for increasing the fluorescence intensity and for controlling the radiation pattern of such radiation are needed.

The question of the control of spontaneous emission of a QE was first addressed by Purcell [9], who considered how the spontaneous emission probability could be increased for an atom in the resonator such that the frequency of its single mode is tuned to the atomic transition frequency. In [9], Purcell showed that the spontaneous relaxation rate of a magnetic dipole in a resonator can increase compared with the relaxation rate in free space, which means that the environment substantially changes the radiative properties of an atom. Both the nanoresonators considered by Purcell and nanoantennas can be used as the nanoenvironment. An important advantage of antennas compared with resonators is their wide frequency band.

According to the Purcell formula for a single-mode resonator, the increase in the fluorophore emission rate in a dielectric resonator compared with the emission rate in a vacuum is described by the coefficient

$$F = \frac{3}{4\pi^2}\,\lambda^3\,\frac{Q}{V}\,, \tag{9}$$

where Q is the quality of the resonator mode and V/λ^3 is the volume of the mode expressed in cubic wavelengths.

Microresonators can support modes of an extremely small volume, which directly leads to a requirement for large Q ($Q > 10^4$). Hence, the greater the Purcell factor we want for a nanoresonator, the less the linewidth and the more difficult the process of tuning the resonator for a specific QE. In

addition, a large Q implies a slow (picosecond or nanosecond) response, which ultimately can obstruct superfast switching. Nanoantennas, as opposed to nanoresonators, are open broadband systems, typically with $Q = 3-30$. An increase in the emission rate can occur across the entire QE spectrum (e.g., an organic dye or quantum dot). Hence, given the need to ensure a small volume of the mode, the electromagnetic energy is to be stored in a material resonance. Single-photon nanoantennas are therefore manufactured from plasmon or polariton ones and recently, due to the development of the technologies, also from hybrid (metal–dielectric) materials.

We note that Q and V in (9) are not defined for plasmonics [67, 68]; if frequency is used as an eigenvalue, then the eigenfunctions increase without bounds at infinity, which leads to complications in numerically solving partial differential equations. In this review, we use another approach (see Section 2), where the dielectric permittivity is used as an eigenvalue, the eigenfunctions decrease at infinity, and all values are well defined for any system.

Before discussing the modification of the spontaneous relaxation rate near nano-objects, we note that the theory of the interaction of an atom with the field deals with two distinct regimes: strong and weak coupling. The difference between these regimes is determined by the atom–field coupling constant

$$\varkappa = d\sqrt{\frac{\hbar\omega_0}{2\varepsilon_0\varepsilon_\mathrm{r}V}}\,, \tag{10}$$

where ω_0 is the atomic transition frequency, d is the dipole matrix element, ε_0 is the dielectric permittivity of the vacuum, ε_r is the relative dielectric permittivity, and V is the resonator volume. The weak coupling regime is determined by the condition $\varkappa \ll \gamma$, and the strong coupling one, by $\varkappa \gg \gamma$, where γ is the photon relaxation rate in the resonator.

In the weak coupling regime $\varkappa \ll \gamma$, the eigenstates of the coupled system coincide with the unbound system eigenstates, and the spontaneous emission rate can change significantly due to changes in the local density of states (see Section 3.2). In the strong coupling regime $\varkappa \gg \gamma$, the interaction is quite strong, such that not only the spontaneous emission rate but also the energy levels of the system change. Excited QEs and electromagnetic modes reversibly and coherently exchange energy in the resonator at a high rate $\varkappa$. The energy levels of the hybrid system are very different from those of the QE and the electric field taken separately. This leads to a splitting of the QE spectral response, known as Rabi splitting [69].

In the weak coupling regime, the classical theory and calculations within quantum electrodynamics (QED) yield the same result for the modified rate of spontaneous emission relaxation. In the strong coupling regime, the spontaneous decay of an atom, as shown in [70–73], is also described well within the classical approach. But in terms of classical theory, spontaneous relaxation is modified due to the scattering of atomic fields on the environment, whereas in the QED framework relaxation is partly due to vacuum field fluctuations, which in turn depend on the environment. We consider the classical and quantum approaches to the description of spontaneous QE relaxation in the presence of an NP.

3.1 Classical approach

We consider spontaneous relaxation in the framework of the classical approach [74], modeling the QE with a free dipole oscillating in accordance with the harmonic law. The dipole equation of motion in free space is

$$\frac{\mathrm{d}^2\mathbf{d}(t)}{\mathrm{d}t^2} + \gamma_0\frac{\mathrm{d}\mathbf{d}(t)}{\mathrm{d}t} + \omega_0^2\mathbf{d}(t) = 0\,, \tag{11}$$

where $\mathbf{d} = \Delta\mathbf{r}$ is the electric dipole moment of the oscillator and ω_0 is its eigenfrequency. The spontaneous decay rate in the vacuum is defined as

$$\gamma_0 = \frac{1}{4\pi\varepsilon_0}\,\frac{2e^2\omega_0^2}{3mc^3}\,. \tag{12}$$

If the oscillator is located near an NP, it is acted upon by an additional field $\mathbf{E}_\mathrm{s}(\mathbf{r}_0, t)$, absent for the oscillator in a homogeneous space, and the equation of motion becomes

$$\frac{\mathrm{d}^2\mathbf{d}(t)}{\mathrm{d}t^2} + \gamma_0\frac{\mathrm{d}\mathbf{d}(t)}{\mathrm{d}t} + \omega_0^2\mathbf{d}(t) = \frac{e^2}{m}\,\mathbf{E}_\mathrm{s}(\mathbf{r}_0, t)\,. \tag{13}$$

To find the reflected field $\mathbf{E}_\mathrm{s}(\mathbf{r}_0)$, we must solve the full system of Maxwell equations where the charge and current originate from the oscillator dipole moment. The expression for the change in the spontaneous decay rate, called the *Purcell factor*, is

$$\frac{\gamma}{\gamma_0} = 1 + \frac{6\pi\varepsilon_0}{|d_0|^2}\,\frac{1}{k^3}\,\mathrm{Im}\left[\mathbf{d}_0\mathbf{E}_\mathrm{s}(\mathbf{r}_0, \omega_0)\right], \tag{14}$$

where $\mathbf{d}_0$ is the oscillator dipole moment in the vacuum. The resulting expression is also applicable in the case of complex permittivity, i.e., in the case of losses in matter.

The change in the QE spontaneous emission rate in the presence of an NP was first studied in [75, 76], where it was shown that the radiative part of the decay rate has the form

$$\frac{\gamma}{\gamma_0} = \frac{|\mathbf{d}_\mathrm{tot}|^2}{|\mathbf{d}_0|^2}\,, \tag{15}$$

where $\mathbf{d}_\mathrm{tot}$ is the total dipole moment of the QE + NP system. This formula is applicable to any NPs, including those with losses.

3.2 Quantum approach

In the QED framework, spontaneous relaxation is described by considering the interaction of a QE with the continuum of states. In the simplest case, we describe the QE by a two-level system with the ground state $|\mathrm{g}\rangle$ and the excited state $|\mathrm{e}\rangle$, with the transition frequency ω_0 and the dipole transition moment $\mathbf{d}$. According to Fermi's golden rule, the spontaneous relaxation rate can be expressed as

$$\gamma = \frac{2\pi}{\hbar}\sum_f \left|\langle f|\hat{H}_I|i\rangle\right|^2\rho_\mathbf{d}(\mathbf{r}_0, \omega_0)\,, \tag{16}$$

where $\hat{H}_I = -\hat{\mathbf{d}}\hat{\mathbf{E}}$ is the interaction Hamiltonian in the dipole approximation. We here consider combined states of the field and the system, and transitions from the initial excited state $|i\rangle = |\mathrm{e}, \{0\}\rangle$ with energy E_i to the set of final states $|f\rangle = |\mathrm{g}, \{1_{\omega_k}\}\rangle$ with energy E_f for any of these states. The final states differ only in the radiation field mode k. The number of individual single-photon states is determined by the partial local density of states $\rho_\mathbf{d}(\mathbf{r}_0, \omega_0)$, where $\mathbf{r}_0$ determines the position of the two-level system.

The expression for the spontaneous relaxation rate in terms of the Green's function, whose detailed derivation can

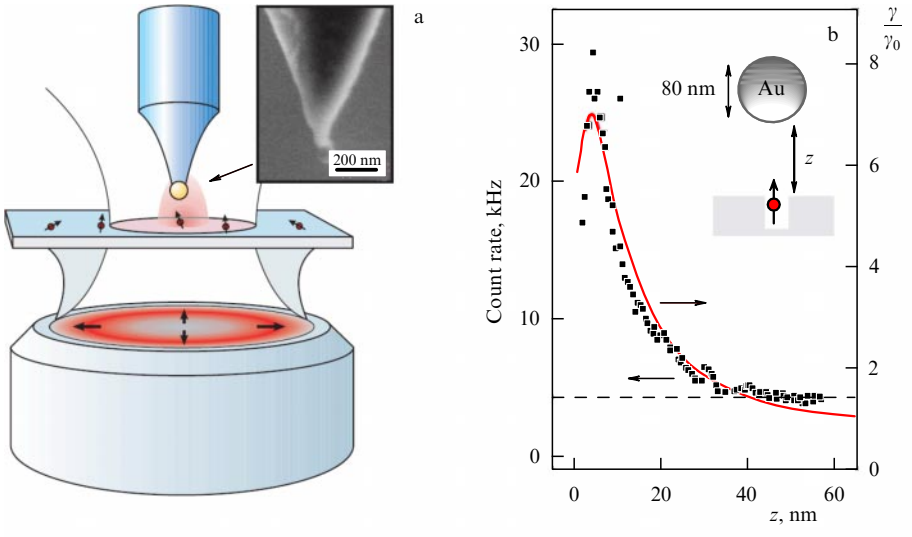

Figure 3. (Color online.) Effect of a gold NP fixed at the tip of a scanning microscope on the fluorescence of a single nile blue dye molecule: (a) scheme of the experiment, (b) experimental (symbols) and theoretical (curve) dependences of fluorescence intensity on distance between nanoantenna and dye molecule [87].

be found in book [32], is

$$\gamma = \frac{2\omega_0}{3\hbar\varepsilon_0 c^2}\,|\mathbf{d}|^2\rho_{\mathbf{d}}(\mathbf{r}_0,\omega_0)\,, \qquad (17)$$
$$\rho_{\mathbf{d}}(\mathbf{r}_0,\omega_0) = \frac{6\omega_0}{\pi c^2}\,\mathbf{n}\,\mathrm{Im}\,\mathbf{G}(\mathbf{r}_0,\mathbf{r}_0,\omega_0)\mathbf{n}\,,$$

where the dipole moment is represented by the product $\mathbf{d} = d\mathbf{n}$, with $\mathbf{n}$ being the unit vector in the direction of $\mathbf{d}$. This formula allows calculating the spontaneous relaxation rate for a two-level quantum system for closed lossless resonators, where the notions of a mode and its eigenfrequency are well defined if the Green's function for the environment is known. The spontaneous relaxation rate is expressed in terms of the partial local density of states ρ corresponding to the number of modes per unit volume and frequency, in a point-like quantum system with the coordinate $\mathbf{r}_0$, in which a photon with the energy $\hbar\omega_0$ can be emitted in the course of spontaneous relaxation; $\rho_{\mathbf{d}}$ is called the partial local density of optical states (PLDOS).

We note that expression (17) for the total relaxation rate of a QE is valid in the presence of arbitrary losses in the environment in both the classical and quantum formulations of the problem [77, 78]. In the case of a lossless NP, the quantum mechanical approach usually allows obtaining the result more straightforwardly, because it is readily expressed as a relatively simple expansion in solutions of the homogeneous Maxwell equations. In [79–81], the quantization procedure for electromagnetic fields was generalized to the case of dispersive and absorbing media. In the framework of that theory, the equivalence of classical and quantum results for the spontaneous transition frequencies in the first order of the perturbation theory has been shown.

When the environment is homogeneous and isotropic, spontaneous relaxation rate (17) is averaged over all possible orientations, and the partial local density of states $\rho_{\mathbf{d}}$ becomes identical to the total local density of optical states (LDOS) defined as

$$\rho(\mathbf{r}_0,\omega_0) = \frac{2\omega_0}{\pi c^2}\,\mathrm{Im}\left(\mathrm{Tr}\left(\mathbf{G}(\mathbf{r}_0,\mathbf{r}_0,\omega_0)\right)\right). \qquad (18)$$

Experimental work on studying the influence of the nanoenvironment on the process of spontaneous relaxation was started as early as the 1960s. The first experimental verification of the influence that the interface between media has on the spontaneous relaxation of molecules was carried out in 1966 in [82] and then 17 years later in [83]. Importantly, the nanoenvironment can increase as well as decrease the relaxation rate [84]. An inhomogeneous environment also affects the nonradiative energy transfer by adjacent molecules (the so-called Förster energy transfer [85]).

The concept of an optical nanoantenna with a single fluorophore as the active element and with optical excitation was first proposed in 2000 [86]. In the early 2000s, researchers used single fluorescent molecules as point-like probes to quantify the electromagnetic field concentration near the tip of a scanning microscope. It was shown that the radiation pattern of a single molecule can be strongly modified by a metallized probe, which essentially acts as a plasmonic nanoantenna.

In 2006, two groups [87, 88] independently studied the change in the fluorescence of a nile blue dye molecule depending on the distance to a spherical gold NP, 80 nm in diameter, fixed on a scanning microscope tip. The results of measurements and theoretical calculations shown in Fig. 3 demonstrate that, as the NP comes closer to the molecule, the fluorescence intensity first increases by a factor of 30 and then is quenched due to the predominance of nonradiative processes.

The experiments clearly demonstrated three fluorescence amplification factors that occur for any optically controlled nanoantenna; their product determines the count rate of single fluorescent photons emitted by a QE, and each of these factors contributes to the change in the electromagnetic field around the antenna:

$$I(\mathbf{r},\omega_{\mathrm{pump}},\omega_{\mathrm{em}}) \propto P_{\mathrm{pump}}(\mathbf{r},\omega_{\mathrm{pump}})\varphi(\mathbf{r},\omega_{\mathrm{em}})C_{\mathrm{NA}}(\mathbf{r},\omega_{\mathrm{em}})\,. \qquad (19)$$

Here, the argument $\mathbf{r}$ emphasizes the dependence of the intensity on the location of the QE, ω_{pump} is the pump

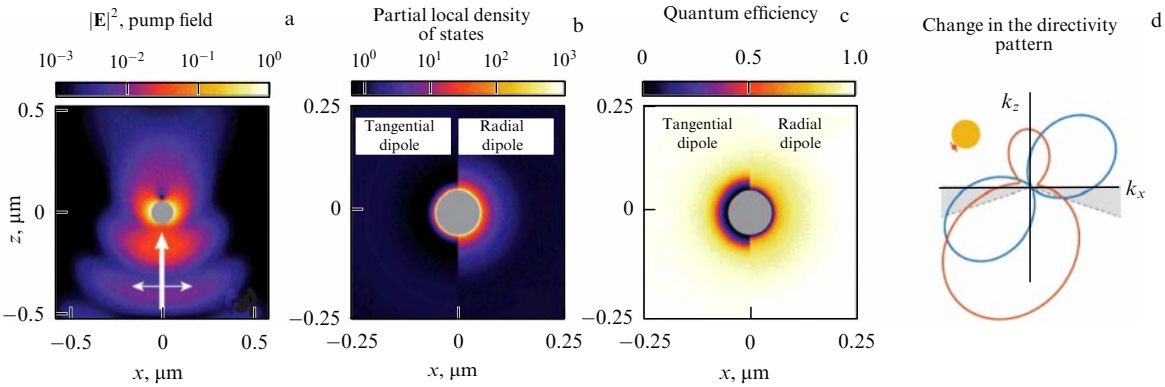

Figure 4. (Color online.) All factors affecting the fluorescence amplification in optically controlled nanoantennas are strongly dependent on the position near the nanoantenna. Example of a gold spherical NP 100 nm in size placed in water and excited by a narrow (NA = 1.3) laser beam at a wavelength of 567 nm; emission is at a wavelength of 600 nm. (a) Distribution of the pump field (first term in (19)) for a wave incident from below and polarized along the *x*-axis. (b) Partial local density of states near the same Mie sphere (at radiation wavelength of 600 nm) strongly increases on the surface of the metal, especially for radial dipole moments of the transition. (c) Quantum efficiency of emission (second term in (19)) under the condition that the intrinsic QE efficiency strongly decreases in a shell 10 nm in radius around the metal. (d) Example of emission redistribution, in this case, for a QE (shown in the upper part), very close to the NP surface and at a distance of 10 nm from the NP, in the *xz* plane (arbitrarily chosen geometry). Directivity pattern is shown as a polar graph for a free QE (blue curve) and a QE near the NP (orange curve). Area shaded in gray shows the boundaries of a typical acceptance cone for a camera lens with a high numerical aperture. Depending on the geometry, collection probability can vary greatly (third term in (19)). (Figure adapted from [90].)

frequency, ω_{em} is the fluorescence frequency, and C_{NA} is the probability of detecting the emitted photon. Figure 4 illustrates these factors for a metal nanosphere. We note that a linear dependence of the fluorescence intensity on pumping is assumed in (19), which is the case only at low pumping intensities [89], as in most experiments with single QEs.

The first factor P_{pump} (Fig. 4a) corresponds to the enhancement of a single fluorophore excitation and depends on the scattering properties of the antenna at the pump wavelength. Once the molecule is excited, other factors become relevant. The collected signal depends on the *quantum efficiency* $\varphi(r)$, i.e., on the probability that the QE excitation results in the emission of a photon.

The excitation energy of any quantum system dissipates either radiatively with the emission of photons or nonradiatively, for example, due to quenching by the surrounding atoms or molecules. The relaxation rate is the sum of the radiative and nonradiative rates γ_r and γ_{nr}. In fluorescence enhancement experiments, the maximum QE *quantum efficiency*, or *quantum yield*, $\varphi(r) = \gamma_r/(\gamma_r + \gamma_{nr})$ had to be achieved. In a homogeneous medium, the quantum efficiency $\varphi(r)$ is identical to the intrinsic quantum efficiency φ_0, whose value lies in the range from 0 to 1, and the parameter itself determines the fraction of energy losses associated with radiation. Inhomogeneities lead to a change in γ_r and γ_{nr}, because they are functions of the local environment. A particular medium can either increase or decrease the quantum efficiency (Fig. 4c). The change in the quantum efficiency is determined by the PLDOS, whose dependence on the orientation of the dipole near a gold nanosphere is shown in Fig. 4b.

We note that any effect that the PLDOS has on the QE spontaneous emission rate in an arbitrary nanoenvironment is often referred to as the 'Purcell gain,' although Purcell himself never considered any system other than a resonator. But the term 'Purcell gain' has become common in the literature, and is often used synonymously with PLDOS.

In addition to changing the quantum efficiency, nanoantennas can also considerably change the radiation pattern (Fig. 4d). Creating an antenna with a given radiation pattern leads to an increase in the efficiency of collecting fluorescence photons by an optical system within a specific solid angle in the far field.

The effects of fluorescence emission amplification listed above determine the list of main problems that have to be solved when creating single-photon nanoantennas with an optical drive.

(1) Controlling the pump gain, the quantum efficiency, and the directivity enhancement effects for significant gains in performance.

(2) Controlling the positioning and orientation of individual QEs and antennas with nanometer precision.

(3) Working out the antenna–emitter geometry to ensure the required radiation pattern.

3.3 Studies of quantum emitters near a nanoparticle and on substrates

Experimental studies of single QEs are extremely complex. Studied in the first experiments were the lifetimes of atoms and ions, in particular, the Eu^{3+} ion, located near a partially reflecting planar surface [91, 92]. This geometry allows carrying out exact theoretical calculations within both classical [91, 93] and quantum [94] approaches. A comparison of theoretical and experimental results showed their good agreement.

Subsequently, a large number of papers were published on the study of spontaneous QE emission near NPs of specific geometries: spherical [95, 96] and an infinite circular ideally conducting cylinder [97–101]. In [75], the simple asymptotic form was obtained for an atom located on the surface (radial orientation) of a dielectric cylinder with a subwavelength size.

Of particular interest are NPs of spheroidal geometry, because the influence of a spheroid on the spontaneous emission of a QE is intermediate between the cases of a sphere and a cylinder and allows effectively controlling both radiative and nonradiative decay rates for an excited QE state. Controlling the geometric size of the nanospheroid — the ratio of the semiaxes b/a — allows 'tuning in' to the plasmon resonances of a particular substance.

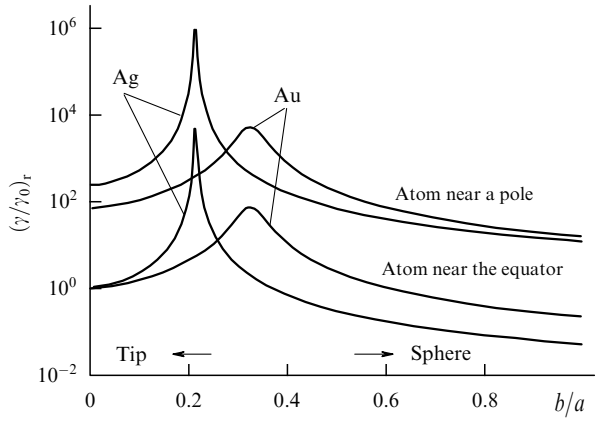

Figure 5. Dependence of spontaneous transition frequencies near an NP in the shape of nanospheroids made of gold ($\varepsilon = -8.7 + i1.16$, $\lambda = 600$ nm) and silver ($\varepsilon = -15.7 + i0.21$, $\lambda = 62.8$ nm) on the ratio b/a of spheroid axes for the dipole orientation parallel to a spheroid axis [34].

A significant acceleration of spontaneous decays near a nanospheroid in the case of plasmon resonance (Fig. 5) can be used as the basis for the operation of an aperture-free scanning microscope with an individual molecule as an object. In such a microscope, the tip can be approximated by a prolate nanospheroid in which plasmon resonance can be excited at the molecular radiation frequency. The absorption band of the molecule is assumed to be far from the plasmon resonance. Calculations performed in [102, 103] showed that a microscope of this kind allows determining both the position of a molecule and the orientation of its dipole moment with nanometer resolution.

A conical surface can serve as another model of a microscope tip. Theoretical calculations of the spontaneous QE decay rate near such a surface were carried out in [104, 105].

A large number of plasmonic nanoantennas that can significantly enhance the near field do not lead to an effective increase in QE fluorescence. It may be natural to speak of 'dark' plasmonics when nonradiative decay channels dominate, and 'light' plasmonics when the radiative decay channel dominates. A classification of different types of antennas that produce bright plasmon-enhanced radiation (Fig. 6) is given in [90].

For dipole antennas (Fig. 6a) such as nanorods [106] and dimer antennas with gaps [107–109], amplification up to 1000 times has been reported, with the fluorescence brightness increasing in equal parts due to an increase in pumping and in the LDOS. A detailed description of spontaneous QE emission near dipole nanoantennas of the most general form (nanoellipsoids) is given in [110, 111], and near disks, in [28, 112, 113].

An array of phased NPs [114] or antennas in the form of an arrangement of nanoholes [115, 116] (Fig. 6b) allows controlling the radiation directivity, but typically leaves the Purcell factor rather low. Strip antennas [117, 118] (Fig. 6c) allow obtaining a high LDOS. Radiation through the edges is directional, depending on the size of the inclusions.

Nanoresonators integrated with quantum dots (QDs) [119] are another type of antenna that increase the overall radiation intensity by about 2×10^3 times. Such antennas have a versatile geometry into which many other QEs can be integrated, including NV (nitrogen-substituted vacancy) centers.

Dielectric antennas at frequencies close to the multipole resonances also allow obtaining a pronounced directivity pattern [120–122] and can cause a considerable increase in fluorescence brightness [123], but make an significant increase in the Purcell factor much more difficult to achieve [124].

As we have noted, so-called hybrid nanoantennas are being studied more and more actively. For example, in theoretical study [109], the concept of a hybrid metal–dielectric 'butterfly' nanoantenna was proposed. Such a nanoantenna is a traditional butterfly-shaped plasmonic nanoantenna whose tips are made of diamond containing an NV center. NV centers in diamond are promising candidates for the role of QEs due to the simple structure of their energy levels and the possibility of controlling the electron spins of the centers by means of microwave radiation and, as a result, modulation of the absorption and luminescence spectra.

The authors of [109] showed that the volume of the mode in such a nanoantenna is very small and the electric field is concentrated at the center of the butterfly, where the NV centers are accumulated. This increases the Purcell factor to values of the order of 110 and also increases the emitted photon collection efficiency by a factor of 1.77.

Asymmetric hybrid dimeric nanoantennas consisting of metal and silicon spherical NPs (Fig. 7a), called Janus dimers, were studied in [125]. The radiation patterns of such antennas were studied in detail, and it was shown that suppression of the back lobe of the radiation pattern is achieved due to the destructive interference of optical waves scattered on the magnetic dipole moment of the dielectric nanosphere and waves scattered on the electric dipole moment of the metal nanosphere. Because of the relatively

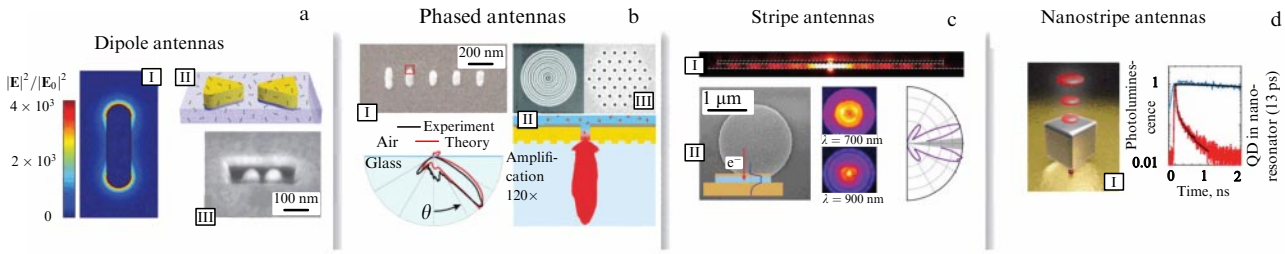

Figure 6. (Color online.) Single-photon nanoantennas. (a) Nanorod dipole antennas and dimer/slot antennas. They have been reported to cause a 1000-fold increase in fluorescence brightness for inherently poor emitters in equal parts by pumping and improving the LDOS. (b) Phased NP or apertured antennas change the emission directivity, usually with poor control of the Purcell factor. (c) Stripe antennas are metal–insulator–metal waveguides for obtaining high LDOSs. Radiation leakage at the edges is directional and dependent on the size of the region. (d) Stripe metallic-NP–dielectric–metal nanoantennas, according to the literature, show more than a 500-fold increase in the Purcell factor and an almost 2000-fold increase in brightness even for very good emitters. Although such an antenna is directional to some extent, it is difficult to control. (Figure adapted from [90].)

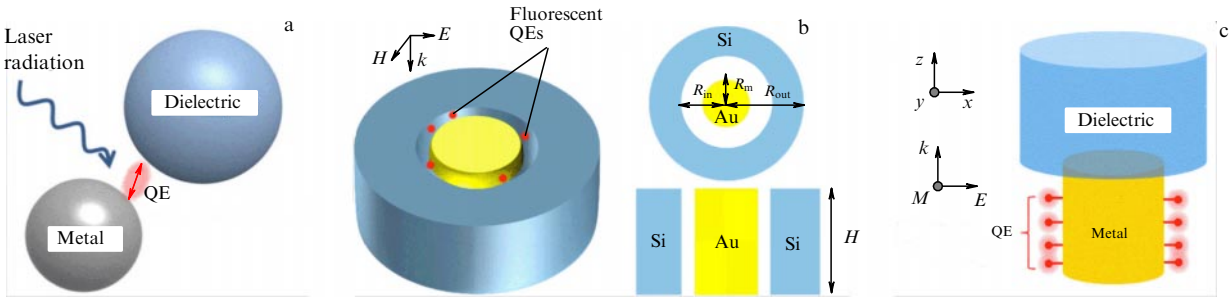

Figure 7. (Color online.) (a) Asymmetric hybrid dimer nanoantenna consisting of spherical metal and silicon NPs. (b) More complex hybrid antenna consisting of an inner metallic (Au) nanodisc and an outer dielectric (Si) hollow cylinder. (c) Mushroom-shaped hybrid antenna made of metal and dielectric nanocylinders.

small spectral width of the magnetic dipole mode, unidirectional scattering has a narrow-band character. The authors showed that unidirectional scattering is enhanced when arranging a large number of Janus dimers into chains, which is explained by additional interference of waves scattered by neighboring dimers, such that light scattering in the lateral and backward directions disappears and radiation in the forward direction is enhanced.

Multiple amplification of the electric field occurs in the gap of such a dimer, which can be used to excite energy transitions of fluorescent molecules and other QEs. A detailed analytic study of all properties of such a nanoantenna beyond the dipole–dipole approximation, which loses its applicability at small distances between nanoparticles, was carried out in [28, 112, 113, 126, 127]. There, spontaneous decay rates for an excited state of a QE located near a cluster of two NPs (nanospheres) made of an arbitrary material with an arbitrary mutual arrangement were investigated in the quasistatic approximation. The constructed theory allows finding the decay rates for various orientations of the dipole moment and QE positions relative to the cluster. It was shown that the decay rates increase significantly at resonance frequencies corresponding to the plasmon oscillation frequencies in the cluster, which are determined by the mutual arrangement of the NPs. The greatest increase in the spontaneous decay rates occurs for QEs located in the center of the cluster, at small distances between the NPs. It has been established that changing the distance between cluster NPs allows effectively controlling the spontaneous decay rate for a QE located between the NPs. The radiation frequency shift was studied for a QE that is located at an arbitrary point, is arbitrarily oriented with respect to the cluster, and has a dipole moment in the general case. Asymptotic expressions for both the spontaneous decay rates and the frequency shift have been discussed. It was shown that, when the distance between the NV centers of the same NP exceeds eight of their radii, the main contributions to the characteristics under study can be calculated within a model where the spheres are replaced with point dipoles whose polarizabilities are equal to the polarizabilities of each of the spheres in a uniform field.

Recently, in [128], the change in the radiative and nonradiative decay rates for a QE (an electric or magnetic dipole) located in the gap of such a dimer has been discussed, depending on the orientation (along or across the dimer axis) of the unit dipole and on the resonance excited in the dipole NP. The potential of a hybrid dimer used as an antenna for amplifying fluorescence radiation was also studied. In this case, the QE was modeled as a statistical ensemble of randomly oriented dipoles located along the dimer axis. Three variants of dimers were considered: metal–dielectric, metal–metal, and dielectric–dielectric. The radiative decay rates γ_{ext}/γ_0, the averaged quantum yield $\langle q/q_0\rangle$, and the average fluorescence emission gain $\langle\eta_{em}/\eta_0\rangle$ were calculated for them.

Calculations showed that, because the hybrid dimer combines both metallic and dielectric NPs, the corresponding fluorescence excitation rate and the average quantum yield are naturally limited by values intermediate between those for systems of purely metallic and dielectric dimers. However, the final enhancement of the fluorescence emission depends on the product of the radiative decay rate and the yield, and hence the hybrid dimer allows a better balance to be achieved between the fluorescence excitation rate and the quantum yield. Ultimately, $\langle\eta_{em}/\eta_0\rangle = 87$ for the hybrid dimer, which is 30% higher than for the pure dielectric dimer ($\langle\eta_{em}/\eta_0\rangle = 67$), and very close to the value for a metal dimer ($\langle\eta_{em}/\eta_0\rangle = 90$).

In [129], a hybrid antenna with a more complex shape was considered, consisting of an inner metallic (Au) nanodisc and an outer dielectric (Si) hollow cylinder (Fig. 7b). Unlike a hybrid dimer of two nanospheres, this antenna allows choosing the geometric size such that the increase in the QE fluorescence intensity in the antenna gap is three orders of magnitude greater ($FE_{tot}/(FE_0) > 1500$) than the QE radiation intensity in free space. It has also been shown that the QE fluorescence intensity near the hybrid metal–dielectric antenna is two orders of magnitude higher than for the QE located near only the metal or only the dielectric parts of such an antenna. The important problem of finding the optimal location of the QE relative to the nanoantenna such that the radiative decay rate is maximal and the fluorescence quenching effect minimal was studied in detail in [129].

A mushroom-shaped hybrid antenna was considered in [130] (Fig. 7c). 'Mushroom' nanoantenna resonances can be flexibly tuned to arbitrary wavelengths, so as to match the Stokes shifts in a wide range of fluorescent QEs. The excitation wavelength can be conveniently controlled by changing the material and morphology of the metal stem, because the resonant properties are well preserved in the structure of the mushroom, while the emission wavelength is easily controlled by changing the morphology of the dielectric cap, which can be observed directly in the spectra. These two examples are illustrated in Fig. 7. When changing the stem material from Ag to Au, the excitation wavelength was retuned from 425 to 520 nm, as shown in Fig. 7a, which corresponded to the resonant property of an isolated Au cylinder. The field distribution is shown in Fig. 7b. By simply changing the size of the Si cylindrical cap, the magnetic dipole

resonances can be located in the range of 590–715 nm in order to correspond to different QE emission wavelengths, as shown in Fig. 7c.

4. Quantum optics of a quantum emitter in the near field of a nanoparticle

Let us consider the quantum optics effects for a system made of a QE placed in the near field of a plasmonic NP in an external electromagnetic field. The mechanisms for modifying the radiative and nonradiative decay rates in the simplest model of a two-level QE located in the immediate vicinity of the plasmonic NP, as well as the distribution of the intensity and polarization of the near field around the NP, were discussed in detail in Section 2. Here, we consider the (NP + QE) + external laser field system and discuss the relevant quantum optics effects: modification of the QE resonance fluorescence spectrum in the near field, bunching/antibunching and quantum statistics of photons in the spectrum, the formation of squeezed states of light, and the generation of quantum entangled states in such systems.

4.1 Resonance fluorescence spectrum of a quantum emitter

A demonstrative system to start discussing the effect of an NP on the resonance fluorescence spectrum of a two-level QE is a spherical plasmonic NP. We consider the resonance fluorescence spectrum, rather than, say, the spontaneous fluorescence spectrum, because it is the former that carries information about the quantum properties of the interaction of light with QE + NP. This problem was first solved in [131] (see the inset in Fig. 10 below). The two-level QE is located near the NP at a point with a radius vector $\mathbf{r}_0$; the QE + NP system interacts with a linearly polarized laser field whose linewidth is $\Delta\omega_{\mathrm{L}} = 1$ MHz.

The resonance fluorescence spectrum of a two-level QE in free space consists of three well-separated spectral lines, the Apanasevich–Mollow fluorescence triplet, which was first predicted by Apanasevich in [132, 133] and then by Newstein [134] and Mollow [135]. Resonance fluorescence was studied in detail experimentally in [136]. The energy level structure of a two-level QE ('dressed states') is shown in Fig. 8a, and its resonance fluorescence spectrum is shown in Fig. 8b.

The theory of resonance fluorescence of a single QE is well known; it is presented, for example, in [137] and can be applied to the case of a QE in any environment. It follows from this theory that the spectral density of the fluorescence emitted by the QE (resonance fluorescence) is determined by the normally ordered correlation function $\langle E^{(-)}(\mathbf{r},t)E^{(+)}(\mathbf{r},t+\tau)\rangle$ of fluorescence light at a point $\mathbf{r}$ in the far field, where $E^{(+)}(\mathbf{r},t)$ and $E^{(-)}(\mathbf{r},t)$ are the positive- and negative-frequency parts of the electric field operator:

$$S(\mathbf{r},\omega_{\mathrm{L}}) = \mathrm{Re}\int_0^\infty \mathrm{d}\tau\,\langle E^{(-)}(\mathbf{r},t)E^{(+)}(\mathbf{r},t+\tau)\rangle \exp(\mathrm{i}\omega_{\mathrm{L}}\tau)\,. \tag{20}$$

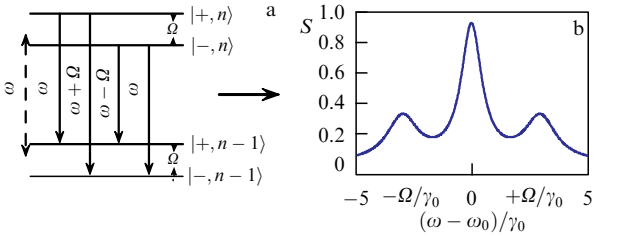

Figure 8. (a) Scheme of split levels of a two-level QE ('dressed' states). (b) Resonance fluorescence spectra of a QE in a strong field in the absence of NPs ($\Omega > \gamma_0$) (Apanasevich–Mollow triplet). Index n shows the energy of the level expressed in photons of the ω field mode.

For a two-level QE, the correlation function is simplified to [137]

$$\begin{aligned}\langle E^{(-)}(\mathbf{r},t)E^{(+)}(\mathbf{r},t+\tau)\rangle &= I_0(\mathbf{r})\sin^2\psi\exp(-\mathrm{i}\omega\tau)\\ &\times\left(\frac{\Omega^2(\mathbf{r})}{\gamma^2(\mathbf{r})+2\Omega^2(\mathbf{r})}\right)\left[\frac{\gamma^2(\mathbf{r})}{\gamma^2(\mathbf{r})+2\Omega^2(\mathbf{r})}+\frac{\exp(-\gamma\tau/2)}{2}\right.\\ &+\frac{\exp(-3\gamma\tau/4)}{4}\Big\{\exp\big(-\mathrm{i}\mu(\mathbf{r})\tau\big)\big(P(\mathbf{r})+\mathrm{i}Q(\mathbf{r})\big)\\ &\left.+\exp\big(\mathrm{i}\mu(\mathbf{r})\tau\big)\big(P(\mathbf{r})-\mathrm{i}Q(\mathbf{r})\big)\Big\}\right],\end{aligned} \tag{21}$$

where $I_0(\mathbf{r}) = [(\omega^2|\mathbf{d}|)/(c^2|\mathbf{r}|)]^2$, Ω is the Rabi frequency, ψ is the angle between the z-axis and the direction of the dipole lying in the yz plane, with the observer assumed to be located on the z-axis, and $P = P(\mathbf{r})$, $Q = Q(\mathbf{r})$, and $\mu = \mu(\mathbf{r})$ are defined as

$$\begin{aligned}P(\mathbf{r}) &= \frac{2\Omega^2(\mathbf{r})-\gamma^2(\mathbf{r})}{2\Omega^2(\mathbf{r})+\gamma^2(\mathbf{r})}\,, \qquad Q(\mathbf{r}) = \frac{\gamma(\mathbf{r})}{4\mu(\mathbf{r})}\,\frac{10\Omega^2(\mathbf{r})-\gamma^2(\mathbf{r})}{2\Omega^2(\mathbf{r})+\gamma^2(\mathbf{r})}\,,\\ \mu(\mathbf{r}) &= \left(\Omega^2(\mathbf{r})-\frac{\gamma^2(\mathbf{r})}{16}\right)^{1/2}.\end{aligned} \tag{22}$$

The effect of the NP is taken into account here via the effective (NP-modified) values of the Rabi frequency and linewidths.

Using the Fourier transform of

$$\langle E^{(-)}(\mathbf{r},t)E^{(+)}(\mathbf{r},t+\tau)\rangle\,,$$

and also taking into account that

$$\int_0^\infty \mathrm{d}\tau\,\exp\left(-\mathrm{i}\omega t-\frac{\gamma\tau}{2}+\mathrm{i}\omega_{\mathrm{L}}\tau\right) = \frac{1}{\mathrm{i}(\omega-\omega_{\mathrm{L}})+\gamma/2}\,, \tag{23}$$

$$\begin{aligned}\int_0^\infty \mathrm{d}\tau\,\exp&\left(-\mathrm{i}\omega t\mp\mathrm{i}\mu\tau-\frac{3\gamma\tau}{4}+\mathrm{i}\omega_{\mathrm{L}}\tau\right)\\ &= \frac{1}{\mathrm{i}(\omega-\omega_{\mathrm{L}}\pm\mu)+3\gamma/4}\,,\end{aligned} \tag{24}$$

we obtain the spectral density $S(\mathbf{r},\omega_{\mathrm{L}})$ of the electromagnetic field at a point $\mathbf{r}$ in the form

$$\begin{aligned}S(\mathbf{r},\omega_{\mathrm{L}}) &= I_0(\mathbf{r})\left(\frac{\Omega^2(\mathbf{r})}{\gamma^2(\mathbf{r})+2\Omega^2(\mathbf{r})}\right)\\ &\times\left[\frac{\gamma^2(\mathbf{r})}{\gamma^2(\mathbf{r})+2\Omega^2(\mathbf{r})}\,\delta(\omega-\omega_{\mathrm{L}})+\frac{\gamma(\mathbf{r})}{(\omega-\omega_{\mathrm{L}})^2}\right.\\ &\left.+\frac{\alpha_+(\mathbf{r})}{\big(\omega+\mu(\mathbf{r})-\omega_{\mathrm{L}}\big)^2}+\frac{\alpha_-(\mathbf{r})}{\big(\omega-\mu(\mathbf{r})-\omega_{\mathrm{L}}\big)^2}\right],\end{aligned} \tag{25}$$

where

$$\alpha_\pm = \frac{3\gamma(\mathbf{r})}{4}\,P(\mathbf{r}) \pm \big(\omega\pm\mu(\mathbf{r})-\omega_{\mathrm{L}}\big)Q(\mathbf{r})\,. \tag{26}$$

Equation (25) shows that the resonance fluorescence of a two-level QE in free space typically consists of four components, whose intensities largely depend on the intensity of the control field and all four contributions. The decay rates in this equation determine the width of the corresponding

Lorentzian lines in the spectrum, which consists of three Lorentzian profiles at the frequencies ω_L and $\omega_L \pm \Omega$, and a coherent response at the frequency ω_L.

To calculate resonance fluorescence near the NP, we must recall that the Rabi frequencies and radiative decay rates change. With (3), the modified Rabi frequency in the case of a nanosphere becomes

$$\Omega(\mathbf{r}) = \frac{d}{\hbar}\sqrt{|E_r|^2 + |E_\theta|^2} = \frac{d}{\hbar}\left[\left|E_0 \cos\theta\left(\frac{2a^3}{r^3}\frac{\varepsilon(\omega)-1}{\varepsilon(\omega)+2}+1\right)\right|^2 + \left|E_0 \sin\theta\left(\frac{a^3}{r^3}\frac{\varepsilon(\omega)-1}{\varepsilon(\omega)+2}-1\right)\right|^2\right]^{1/2}, \quad (27)$$

where d is the QE dipole moment (expressed in Gaussian units), E_0 is the external field amplitude, $\hat{\mathbf{n}}_r$ and $\hat{\mathbf{n}}_\theta$ are unit vectors in spherical coordinates, and $\varepsilon(\omega)$ is the permittivity of the NP at the frequency ω. It is worth noting that, in the case of a sphere, $E_\varphi = 0$.

The total normalized decay rate of a QE located at a point $\mathbf{r}$, with the QE dipole moment oriented along the direction of the local field at that point, can be expressed as

$$\frac{\gamma}{\gamma_0} = \frac{|E_r|^2(\gamma/\gamma_0)_{\text{rad}} + \left(|E_\theta|^2 + |E_\varphi|^2\right)(\gamma/\gamma_0)_{\tan}}{\sqrt{|E_r|^2 + |E_\theta|^2 + |E_\varphi|^2}}, \quad (28)$$

where $(\gamma/\gamma_0)_{\text{rad}}$ is the total decay rate for the radial orientation of the QE dipole moment, which can be expressed as

$$\left(\frac{\gamma}{\gamma_0}\right)_{\text{rad}} \xrightarrow{|\mathbf{k}|a\to 0} \frac{3}{2(|\mathbf{k}||\mathbf{r}|)^3}\,\text{Im}\sum_{n=1}^{\infty}(n+1)^2\left(\frac{a}{|\mathbf{r}|}\right)^{2n+1} \times \frac{\alpha_n}{a^{2n+1}} + \left|1+\frac{2\alpha_1}{|\mathbf{r}|^3}\right|^2 + O\left(\frac{1}{|\mathbf{k}|a}\right), \quad (29)$$

and $(\gamma/\gamma_0)_{\tan}$ is the total decay rate for the tangential orientation of the dipole moment of an atom,

$$\left(\frac{\gamma}{\gamma_0}\right)_{\tan} \xrightarrow{|\mathbf{k}|a\to 0} \frac{3}{4(|\mathbf{k}||\mathbf{r}|)^3}\,\text{Im}\sum_{n=1}^{\infty}n(n+1)\left(\frac{a}{|\mathbf{r}|}\right)^{2n+1} \times \frac{\alpha_n}{a^{2n+1}} + \left|1-\frac{\alpha_1}{|\mathbf{r}|^3}\right|^2 + O\left(\frac{1}{|\mathbf{k}|a}\right), \quad (30)$$

where α_n are nth-order multipole polarizabilities, generalizing the dipole polarizability for $n = 1$:

$$\alpha_n = a^{2n+1}\frac{\varepsilon(\omega)-\varepsilon_2}{\varepsilon(\omega)+\varepsilon_2(n+1)/n}. \quad (31)$$

The results of calculating the QE resonance fluorescence spectra in free space and near NPs are shown in Figs 9 and 10. Figure 9 shows that, in the limit of a weak incident laser field, the resonance fluorescence spectrum of a two-level QE in free space has only one pronounced line at zero frequency detuning. Placing the NP in close proximity to the QE enhances the local field and affects the Rabi frequency and the QE decay rate such that the resonance fluorescence spectrum is enriched and the Apanasevich–Mollow triplet structure transpires. Adjusting these parameters opens up new possibilities for controlling the properties of an atom using an NP.

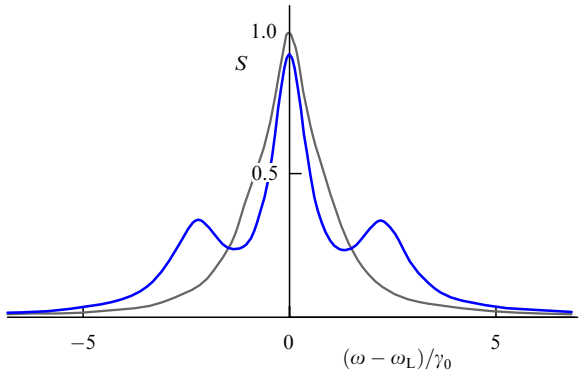

Figure 9. (Color online.) Resonance fluorescence spectrum of a two-level QE. $\gamma_0 = 20$ MHz in free space (lighter curve) and near a spherical NP with radius $a = 20$ nm at a distance of 20 nm from the NP surface (darker curve), with $\theta = 0.3$ rad (17°) in a weak laser field; $\lambda = 632.8$ nm and $\Omega = 0.8\gamma_0$, $E_0 = 500$ V m^{-1}.

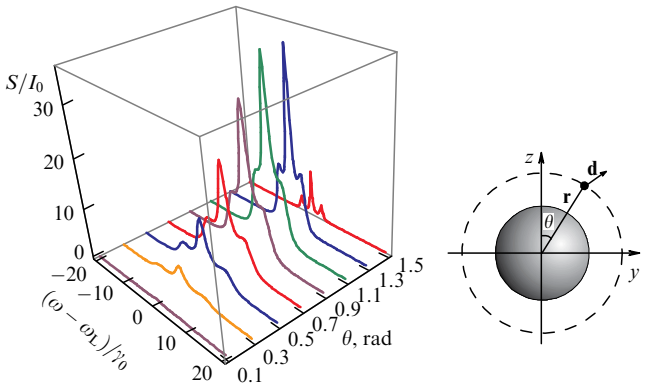

Figure 10. (Color online.) Resonance fluorescence spectrum, normalized to I_0, of a two-level QE located near a spherical NP with radius $a = 20$ nm as a function of angle $\theta = 0.1-1.5$ rad (5.7°–85.9°), at a distance of 10 nm from the QE to the NP surface; $\lambda = 632.8$ nm, $\gamma_0 = 20$ MHz, and $E_0 = 2000$ V m^{-1}.

Figure 10 shows the change in the resonance fluorescence spectrum of a QE, located at a distance of 10 nm from the surface of a nanosphere, depending on the angle θ of the QE position. The resonance fluorescence spectrum depends on the position of the observer as $S \sim \psi^2$, Eqn (25), where ψ is the angle between the QE dipole direction and the z-axis. In this case, the observer is located on the z-axis and the QE dipole moment is oriented in the direction of the local field, such that at the angles $\theta = 0$ and 90° (1.57 rad), the QE resonance fluorescence intensity as seen by the observer at these points in space tends to zero. The local field strength reaches a maximum at $\theta = 0$ and a minimum at $\theta = 90°$, such that, as θ increases, the side lines of the spectrum shift toward the central line due to a decrease in the Rabi frequency. Also note that the resonance fluorescence intensity maximum is observed at $\theta = 1.1$ rad (67°) (see Fig. 10).

The resonance fluorescence spectrum of a two-level QE exhibits a substantial dependence on the distance between the QE and the NP surface at fixed values of the angle θ (Fig. 11). A decrease in the distance between the QE and the NP surface leads to a narrowing of the resonance fluorescence lines and a decrease in the distance between them. At distances of less than 5 nm, the QE nonradiative decay rate is much greater than the radiative decay rate, and hence the so-called fluorescence quenching effect is observed.

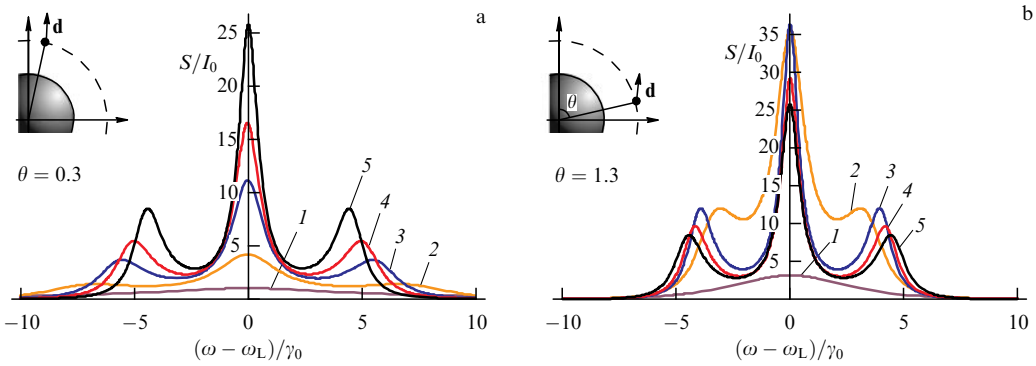

Figure 11. (Color online.) Resonance fluorescence spectrum, normalized to I_0, of a two-level QE located near a spherical NP of radius $a = 20$ nm, for two QE positions: (a) $\theta = 0.3$ rad and (b) 1.3 rad. Distance from the QE + NP system to the surface: 5 nm (curve *1*), 10 nm (*2*), 20 nm (*3*), and 30 nm (*4*); curve *5* corresponds to the QE in free space; $\lambda = 632.8$ nm, $\gamma_0 = 20$ MHz, and $E_0 = 2000$ V m^{-1}.

The approach to the analysis of the interaction between QEs and NPs described above largely relies on the density matrix approximation. We note, however, that a deeper insight into the quantum properties of light emitted by QEs in the presence of NPs can be gained from QED.

In the QED framework, the authors of [73, 138] considered the strong resonant interaction of a two-level QE (atom) with a continuum of quantized electromagnetic modes within the resonance mode of a dielectric microsphere. Analytic solutions were obtained. As the initial condition at the time $t = 0$, the atom was assumed to be excited and the resonance modes of the microsphere assumed to contain a single-photon wave packet. It was shown that the properties of the emitted photon pair depend in a crucial manner on the spatiotemporal properties of the photon wave packet contained in the resonator. If the mean square of the electric field of the photon wave packet at the QE location point is close to the vacuum value at the initial instant, the QE emission is similar to spontaneous emission and the emitted pair of photons is not correlated. Conversely, if the average value of the square of the electric field of the photon wave packet at the QE location is much greater than the vacuum value at the initial instant, then the emission of the atom is stimulated and the emitted photon pair has strong, very intricate correlations. The connection between the obtained results and the predictions of the theory of dressed states was briefly discussed. The results are general and can be applied to describe the strong resonance interaction between a QE and resonators.

In [139], the influence of quantum fluctuations and correlations on the NP dynamics and a two-level QE located in an external optical field was discussed in the approximation of a small number of plasmons. It was shown that, as the coupling constant between the QE and NP increases due to the appearance of Fano resonance, the shape of the Apanasevich–Mollow triplet first becomes asymmetric, then the side maxima disappear, and then the triplet degenerates into a single Lorentzian line.

In addition, it is important to understand the applicability ranges of the quantum and semiclassical descriptions of the systems under consideration. In [140], a detailed quantum mechanical study of the fluorescence spectra of a molecule near a plasmonic NP was carried out. The authors considered both weak- and strong-coupling regimes, as well as the excitation of higher-order modes in the NP, and showed that strong coupling occurs at distances of less than 5 nm and requires a fully quantum mechanical description, while the semiclassical approximation is applicable to the description of the interaction at longer distances.

The two-level QE model is the simplest; more involved QEs have been studied in the literature. For example, in [141], the resonance fluorescence of a three-level Λ-type QE located near a spherical metallic NP was studied. The authors considered the case where the QE is excited by a laser field along one of the optical transitions. It was shown that the spectrum shape depends on the mutual orientation of the dipole moments of optical transitions with respect to the metallic NP surface. It was also shown that the location and width of the peaks in the spectrum are strongly modified by the exciton–plasmon coupling and laser detuning, which allows obtaining a controlled spectral line at the second uncontrolled transition in the Λ system with a width much less than the natural one.

That study was continued in [142], where the resonance fluorescence of a four-level double V-type QE near a plasmonic NP was studied theoretically. The quantum system interacts with two orthogonal circularly polarized laser fields with the same frequency and intensity, but with different phases. A two-dimensional array of metal-coated dielectric nanospheres was considered a plasmonic NP. Spontaneous emission of this QE demonstrates quantum interference near the plasmonic NP. The authors of [142] showed that the presence of the plasmonic NP leads to a strong modification of the resonance fluorescence spectrum. In addition, the resonance fluorescence spectrum and the second-order correlation function are highly phase dependent, and hence the relative phase of the laser fields can be used to effectively control the resonance fluorescence properties.

Some studies have been devoted to the modification of resonance fluorescence spectra for various NPs [143–149]. All these studies are theoretical, however, because the observation of the resonance fluorescence of NP + atom systems is a complex experimental problem, even at the modern level of technology. Among these studies, we note [150]: the QE + NP system was not studied there, but the artificial atom — an interesting and promising subject for quantum computing — was discussed. A Josephson qubit was considered as an artificial atom, and its resonance fluorescence was studied experimentally.

4.2 Photon statistics of the spectrum of resonance fluorescence of a quantum emitter

An important characteristic of resonance fluorescence is the statistics on the distribution of photocounts of fluorescent

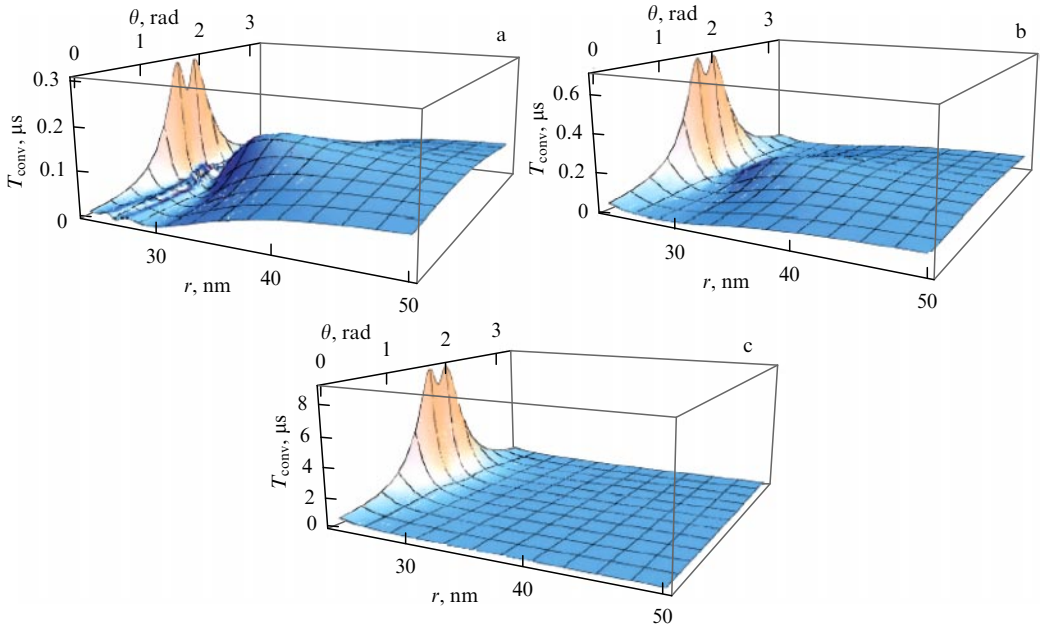

Figure 12. (Color online.) Dependence of the conversion time T_{conv} on the QE coordinates r and θ near an NP for the normalized frequency detuning (a) $D = 0$, (b) $D = 1$, and (c) $D = 5$ with $\Delta\omega_L = 1$ MHz.

photons, which is affected by the presence of an NP near the QE. In [151], statistics on the number of resonance fluorescence photons in a two-level QE near a metal spherical NP excited by a finite-bandwidth laser field was theoretically studied for the first time. The analysis showed that all the interesting physics here is concentrated in a small region around the NP, where the near field and the QE–NP coupling strongly affect the radiative properties of the QE. Estimates show that the size of this region is $r \leqslant 2a$, where r is the distance from the NP center to the QE and a is the nanosphere radius. At longer distances, the influence of the NP disappears and the QE behaves the same as in free space.

Figure 12 shows the behavior of the time T_{conv} of the convergence of the photocount statistics to the Gaussian distribution for a QE located at a point with coordinates r, θ around the NP for three laser detunings D and a finite laser bandwidth $\Delta\omega_L = 1$ MHz. The figure shows that the convergence time significantly depends on the QE coordinates around the nanosphere at distances $r \leqslant 50$ nm for $D = 0$, $r \leqslant 40$ nm for $D = 1$, and $r \leqslant 30$ nm for $D = 5$, which essentially describes the region where the near field of the metal NP is significant. Near $\theta = \pi/2$, the convergence time reaches its global maximum at $r = 23$ nm: $T_{conv}^{max} = 0.3$ μs at $D = 0$ and $T_{conv}^{max} = 9$ μs at $D = 5$, which is two orders of magnitude greater than for a QE in free space, for which $T_{conv} = 0.1$ μs. A typical long-distance convergence time scale, $r > 2a$, tends to the convergence time for free space. There are also two NP-symmetric regions where $\Omega \sim \gamma$ and the convergence time tends to zero. This behavior is determined by the interplay between radiative and nonradiative QE decay rates due to interaction with the metallic NP and the near field.

The distribution function $p(n, T)$ of the probability of emission of n resonance fluorescence photons in a given time interval T depends significantly on the QE location near the NP (Fig. 13), demonstrating a characteristic bend in a comb-like dependence. To identify the origin of this bend, the probability $p(n)$ was calculated for fixed parameters $D = 0$ and $\theta = \pi/6$ for different materials: an ideal-metal (Fig. 13a) and a silver (Fig. 13b) nanosphere. The figure clearly shows that the bending of the $p(n)$ comb dependence is caused by the nonradiative part of the QE decay rate associated with the metallic NP, which is significant in the region $23 \leqslant r \leqslant 40$ nm.

4.3 Antibunching of resonance fluorescence photons of a quantum emitter

The photon antibunching phenomenon [152] for fluorescence radiation of a two-level QE located in free space and excited by a resonance laser field was predicted theoretically in [137, 153, 154] and confirmed experimentally in [3]. The essence of the phenomenon is that there are electromagnetic field states such that $g^{(2)}(0) < g^{(2)}(\tau)$, where $g^{(2)}(\tau)$ is the normalized second-order correlation function

$$g^{(2)}(\mathbf{r}, \tau) = \frac{\langle \hat{\mathbf{E}}^-(\mathbf{r}, t)\hat{\mathbf{E}}^-(\mathbf{r}, t+\tau)\hat{\mathbf{E}}^+(\mathbf{r}, t+\tau)\hat{\mathbf{E}}^+(\mathbf{r}, t)\rangle}{\langle \hat{\mathbf{E}}^-(\mathbf{r}, t)\hat{\mathbf{E}}^+(\mathbf{r}, t)\rangle\langle \hat{\mathbf{E}}^-(\mathbf{r}, t+\tau)\hat{\mathbf{E}}^+(\mathbf{r}, t+\tau)\rangle} . \tag{32}$$

The field is assumed to be statistically stationary and independent of the initial state of the QE, which amounts to assuming that $t \to \infty$.

The second-order correlation function $g^{(2)}(\mathbf{r}, \tau)$ is proportional to the probability of detecting two photons at the point with the coordinate $\mathbf{r}$ within the time interval τ [155, 156]. Photon antibunching is therefore a nonclassical phenomenon in which photon pairs with a time interval $\tau \neq 0$ are detected more frequently than pairs with a zero time interval.

In the case of a stationary field, the normalized second-order correlation function has the form

$$g^{(2)}(\mathbf{r}, \tau) = \frac{\left[\langle \hat{R}_3(\mathbf{r}, \tau)\rangle_G + 1/2\right]}{\left[\langle \hat{R}_3(\mathbf{r}, \tau)\rangle_{ss} + 1/2\right]} , \tag{33}$$

where the index G corresponds to fluorescence radiation of the QE that was initially in the lowest energy state, and the

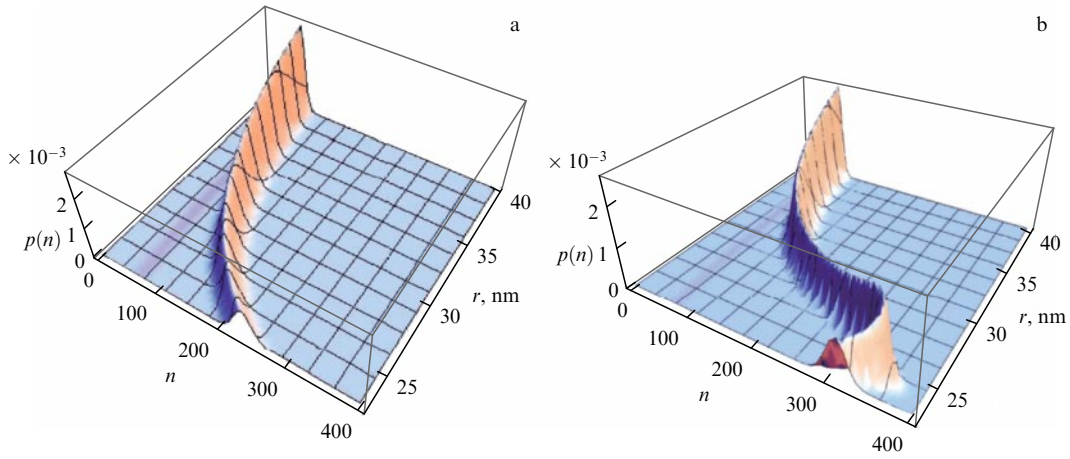

Figure 13. (Color online.) Probability $p(n, T)$ depending on QE coordinate r relative to (a) a spherical NP with $\varepsilon = -\infty$ and (b) a silver NP with $\varepsilon = -15.37 + \mathrm{i}0.231$ at $\theta = \pi/6$ rad, $T = 9$ μs, $D = 0$, $\Delta\omega_{\mathrm{L}} = 1$ MHz, and $\lambda = 632.8$ nm.

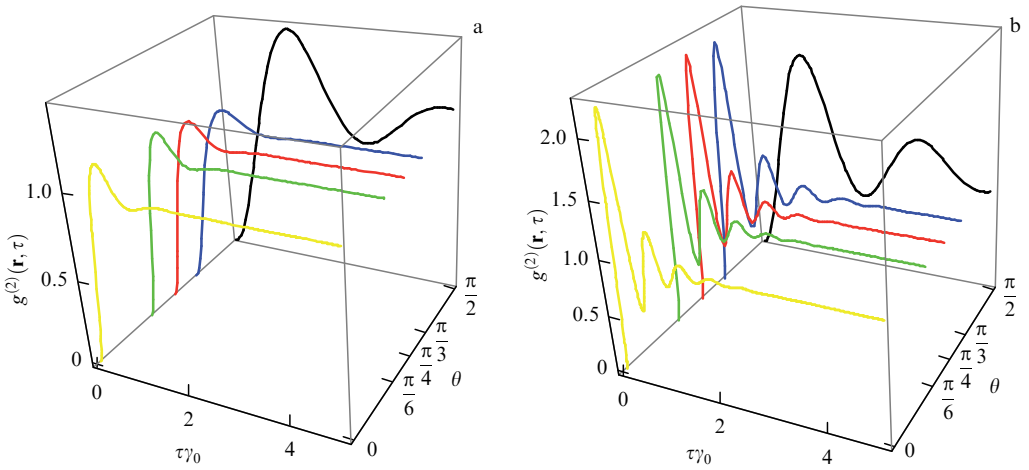

Figure 14. (Color online.) Second-order correlation function $g^{(2)}(\mathbf{r}, \tau)$ for different values of angle θ at a distance of 10 nm to the surface in the case of zero detuning from resonance for laser linewidth (a) $\Delta\omega_{\mathrm{L}} = 0$ and (b) $\Delta\omega_{\mathrm{L}} = 1$ MHz.

subscript ss corresponds to a stationary value ($t \to \infty$) of the Pauli operator $\langle \hat{R}_3(\mathbf{r}, \tau)\rangle$.

For a QE that at the initial instant was in the lowest state, the spin Pauli operator $\langle \hat{R}_3(\mathbf{r}, \tau)\rangle$ has the form

$$\langle \hat{R}_3(\mathbf{r}, \tau)\rangle_{\mathrm{G}} + \frac{1}{2} = \frac{(1/4)\Omega^2(1 + \Delta\omega_{\mathrm{L}}/\beta)}{(1/2)\Omega^2(1 + \Delta\omega_{\mathrm{L}}/\beta) + (\beta + \Delta\omega_{\mathrm{L}})^2 + \beta^2 D^2} - \frac{1}{2}\sum_{i=1,\, i\neq j\neq k}^{3} \frac{(2\beta + p_i)\left[(\beta + \Delta\omega_{\mathrm{L}} + p_i)^2 + \beta^2 D^2\right]\exp(p_i\tau)}{p_i(p_i - p_j)(p_i - p_k)}, \tag{34}$$

where $2\beta = \gamma$ is the QE spontaneous relaxation rate (nonradiative and radiative with the effect of the nanoantenna included), $D = (\omega_{\mathrm{L}} - \omega_0)/\beta$, $\Delta\omega_{\mathrm{L}}$ is the linewidth of the laser radiation incident on the QE–NP system, and p_i, $i = 1, 2, 3$, are the roots of the cubic equation

$$2\beta(\beta + \Delta\omega_{\mathrm{L}})^2 + 2\beta^3 D^2 + (\beta + D)\Omega^2 = 0\,. \tag{35}$$

One of the p_i is a real number and the other two are imaginary complex conjugate numbers [157]. We do not give the expressions for p_i because they are too cumbersome.

The stationary value ($t \to \infty$) of $\langle \hat{R}_3(\mathbf{r}, \tau)\rangle$ is now expressed as

$$\left[\langle \hat{R}_3(\mathbf{r}, \tau)\rangle_{\mathrm{ss}} + \frac{1}{2}\right] = \frac{(1/4)\Omega^2(1 + \Delta\omega_{\mathrm{L}}/\beta)}{(1/2)\Omega^2(1 + \Delta\omega_{\mathrm{L}}/\beta) + (\beta + \Delta\omega_{\mathrm{L}})^2 + \beta^2 D^2}. \tag{36}$$

It follows that $g^{(2)}(\mathbf{r}, \tau)$ depends on the local field strength, the QE spontaneous relaxation rate (radiative and nonradiative), the laser linewidth, and the detuning from resonance at a given point. Therefore, $g^{(2)}(\mathbf{r}, \tau)$ depends on the QE position relative to the nanoantenna.

Figure 14 shows the second-order correlation function $g^{(2)}(\mathbf{r}, \tau)$ for various angles θ and for a 10-nm distance to the surface. It can be seen that $g^{(2)}(\mathbf{r}, \tau)$ depends on the laser linewidth and this parameter cannot be neglected ($\Delta\omega_{\mathrm{L}} =$ 1 MHz in what follows).

Figure 15 shows the correlation function for two values of θ at $r = 30$ nm for various detuning values. It can be seen that $g^{(2)}(\mathbf{r}, \tau)$ depends on the detuning of the QE transition frequency from the resonance. The NP affects the transition frequency. This change is many orders of magnitude smaller than the transition frequency itself, but the expressions for

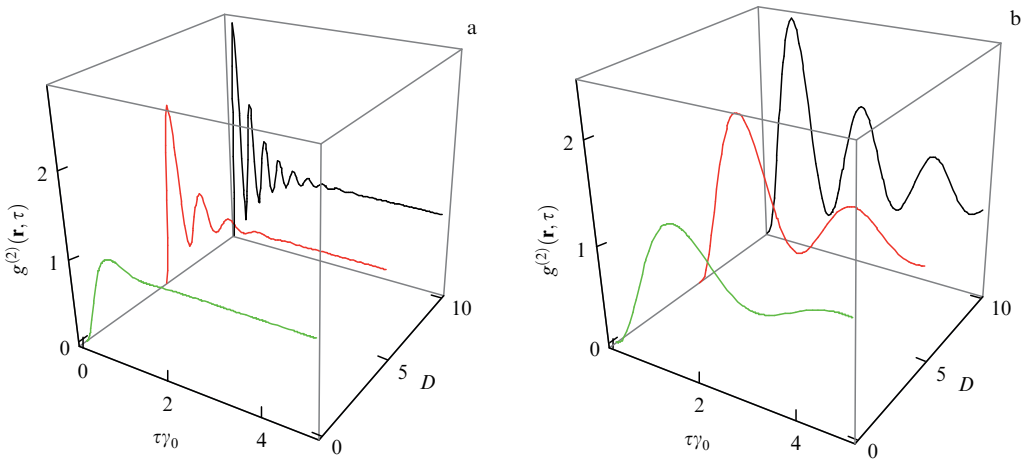

Figure 15. (Color online.) Second-order correlation function $g^{(2)}(\mathbf{r},\tau)$ at $r = 30$ nm for different values of the off-resonance detuning D at (a) $\theta = \pi/4$ and (b) $\theta = \pi/2$.

$g^{(2)}(\mathbf{r},\tau)$ and for the spectral density depend not on the frequency difference but on the ratio $(\omega_L - \omega_0)/\beta$, where $2\beta = \gamma$ is the QE spontaneous relaxation rate (radiative and nonradiative). This ratio is not negligible, even for a resonance detuning equal to several MHz.

The antibunching of fluorescent photons in the case of a Λ-type three-level QE located near a spherical metallic NP was studied in [141]. The authors considered the case where the QE is excited by a single laser field along one of the optical transitions. It was shown that strong antibunching of fluorescence photons is achieved along the second uncontrolled transition in the Λ system.

In [142], the resonance fluorescence of a four-level double V-type QE located near a plasmonic NP was studied theoretically. We consider the case of the interaction of a quantum system with two orthogonal circularly polarized laser fields with the same frequency and intensity, but with different phases. A two-dimensional array of metal-coated dielectric nanospheres is regarded as a plasmonic NP. Spontaneous emission from this QE demonstrates quantum interference near the plasmonic nanostructure. The authors of [142] showed that the presence of a plasmonic NP leads to a substantial modification of both the resonance fluorescence spectrum and the antibunching–bunching transition for fluorescence photons. In addition, the resonance fluorescence spectrum and the second-order correlation function are highly dependent on phase, and hence the relative phase of laser fields can be used to effectively control the resonance fluorescence properties.

In [158], the same authors studied the statistics of two-level QE emission near the same two-dimensional array of metal-coated dielectric nanospheres. It was shown that the statistics on photons are significantly modified by the NP lattice. The antibunching–bunching transition time depends very strongly on the QE orientation with respect to the lattice, the QE transition frequency, the applied electric field strength, and the geometrical parameters of the NP. In particular, for a weakly excited QE whose dipole moment is parallel to the plasmonic lattice, the characteristic antibunching–bunching transition time can increase by two orders of magnitude compared to that in the case of a vacuum in free space. With a stronger external excitation, for a fixed external Rabi frequency, a decrease (or increase) in the antibunching–bunching transition time is observed, when the damping rates decrease (or increase) relative to their values in the vacuum. In addition, the thickness of plasmonic nanoshells can act as a separate control parameter for the photon statistics.

The studies discussed above deal with single QEs. There is currently a growing interest in studying the properties of light generated by hybrid systems that include a mesoscopic number of QEs to create macroscopic quantum light sources. In [159], the statistical properties of light generated by an array of QEs associated with one electromagnetic mode were studied. Theoretical calculations based on the effective Hamiltonian of the system were performed to describe the response of two different systems under low-intensity coherent excitation of plasmonic nanoresonators and dielectric microresonators. Special attention was given to studying the effect that these two types of resonators have on stray light. Starting from an ensemble with the minimum number of QEs equal to one, the stability of photon antibunching upon increasing the ensemble size was analyzed. For both resonator configurations, sub-Poissonian radiation was observed not only at the level of a single QE but also for mesoscopic ensembles consisting of several dozen QEs.

The results show that there are two mechanisms leading to significant negative correlations in the interaction between a purely bosonic subsystem (resonator) and a quasibosonic one (QE ensemble): photon blockade and destructive interference. The first takes place at a high coupling strength (comparable to or greater than the resonator radiation rate), and the second becomes relevant at weaker resonator–QE couplings. Despite the distinctly open or closed nature of these systems and the essentially different physical parameters that describe nanoresonators and microresonators, the photon statistics of both systems have remarkably similar phenomenologies (after normalizing to resonator losses). This can be elucidated by studying the resonator–QE spectral detuning, which increases the range of parameters that give antibunched light, and the time evolution of correlations, showing slow (fast) decay of photon blockade antibunching (induced by interference).

In considering QE–NP systems, the quantum properties of the QE radiation are usually investigated, and the plasmonic NP is regarded as a passive element that alters the local environment of the QE. But in the case of a strong NP–QE coupling, the NP itself can emit light with quantum properties. Unlike the NP in the situation described above, a

metallic NP can emit light in and of itself. Under optical excitation above the onset of interband transitions, noble metal nanoparticles can exhibit rather strong visible photoluminescence. There is experimental evidence that the nonradiative relaxation channel can then include the generation of localized surface plasmons (LSPs), which subsequently emit light. The binding of the metal NP to the QE can lead to an increase in the photoluminescence of the metal NP. On the other hand, LSPs can be excited directly either by fast electrons or by light resonant to the LSP mode. The emission rate of a dipole LSP in a metallic NP is proportional to its volume and can reach values of the order of 10^3 THz, which is three orders of magnitude higher than the limit rate expected for quantum effects associated with metallic nanostructures.

Quantum properties of light emitted by a strongly coupled metallic NP + QE system were studied in [160]. It was shown that such a system effectively behaves like a two-level system and should spontaneously emit light that obeys sub-Poisson statistics and demonstrate ideal antibunching. Two excitation scenarios were considered: (1) a metallic NP is excited nonresonantly via interaction with a three-level QE; (2) a metallic NP + QE system is excited resonantly much below saturation. In the first case, the single-photon generation rate was found to be fundamentally limited by the nonradiative relaxation rate in the excitation channel. The other scenario, on the contrary, is regarded as a simple and promising approach that can provide a repetition rate of single-photon radiation of the order of 100 THz and be used to create single-photon radiation sources.

In real experiments on resonance fluorescence, spectral filtering of resonance fluorescence is widely used to improve the purity and indistinguishability of single photons by removing the unwanted background. The use of this technique, of course, should affect the radiation statistics. It was shown in [161] that the resonance fluorescence spectrum of a two-level QE includes many lines, each of which exhibits different photon statistics. Without filtering, these components always prevent the formation of the strong antibunching expected of a single QE. But with spectral filtering whose bandwidth is comparable to the natural linewidth or the Rabi frequency the ratio of these components changes in the filtered spectrum, leading to substantial changes in the photon statistics.

In the case of weak resonance excitation, a suitable narrow filter removes the incoherent component almost entirely, destroying the antibunching and demonstrating that a subnatural linewidth and strong antibunching cannot be measured simultaneously. With strong resonance excitation, a noticeable bunching effect is observed at filter bandwidths comparable to the natural linewidth before the system eventually tends to the Poisson statistics for the narrowest filters. These results illustrate a possible new approach to controlling the statistics of quantum light photons. It follows that care must be taken to preserve antibunching when filtering the QE spectra.

4.4 Formation of squeezed states of light

We turn to radiation squeezing [152], which is a purely quantum phenomenon, and show that an NP can lead to the squeezing of the fluorescent radiation of a two-level QE located in its near field.

We consider the quadrature squeezing of a fluorescence radiation field. We introduce the Hermitian operators $\hat{\mathbf{E}}_1 = \hat{\mathbf{E}}^+ + \hat{\mathbf{E}}^-$ and $\hat{\mathbf{E}}_2 = -\mathrm{i}(\hat{\mathbf{E}}^+ - \hat{\mathbf{E}}^-)$ for two components of the field strength vector, which differ in phase by $\pi/2$. In this section, for simplicity, field operators are assumed to be normalized to $\omega^2 d/(4\pi\varepsilon_0 c^2|\mathbf{r} - \mathbf{r}_0|)$. In addition, we assume that for each QE position the detector is placed in the far field perpendicular to the QE dipole moment, i.e., $\sin\eta = \pi/2$. We also let

$$[\hat{\mathbf{E}}^+, \hat{\mathbf{E}}^-] = C\,,$$

where C is a function of r and θ, which, taking into account [135, 162, 163], has the form

$$C = \frac{(1 + \Delta\omega_\mathrm{L}/\beta)^2 + D^2}{Z^2(1 + \Delta\omega_\mathrm{L}/\beta) + (1 + \Delta\omega_\mathrm{L}/\beta)^2 + D^2}\,.$$

We then have the commutator

$$[\hat{\mathbf{E}}_1, \hat{\mathbf{E}}_2] = 2\mathrm{i}C\,.$$

Therefore, dispersions of the quantities corresponding to the operators $\hat{\mathbf{E}}_1$ and $\hat{\mathbf{E}}_2$ are [164]

$$\big\langle (\Delta\hat{\mathbf{E}}_1)^2 \big\rangle = C + \big\langle : (\Delta\hat{\mathbf{E}}_1)^2 : \big\rangle\,,$$
$$\big\langle (\Delta\hat{\mathbf{E}}_2)^2 \big\rangle = C + \big\langle : (\Delta\hat{\mathbf{E}}_2)^2 : \big\rangle\,,$$

where the colon denotes normal ordering.

In our case, we have the squeezing condition $\langle : (\Delta\hat{\mathbf{E}}_1)^2 : \rangle < 0$ or $\langle : (\Delta\hat{\mathbf{E}}_2)^2 : \rangle < 0$. We note that there is no classical analogue of a squeezed state. The squeezing conditions for the components $\hat{\mathbf{E}}_1$ and $\hat{\mathbf{E}}_2$ can be expressed as

$$\big\langle : (\Delta\hat{\mathbf{E}}_1)^2 : \big\rangle = 2\big\langle \hat{\mathbf{E}}^-\hat{\mathbf{E}}^+ \big\rangle - \big(\big\langle \hat{\mathbf{E}}^+ \big\rangle + \big\langle \hat{\mathbf{E}}^- \big\rangle\big)^2 < 0\,, \quad (37)$$

$$\big\langle : (\Delta\hat{\mathbf{E}}_2)^2 : \big\rangle = 2\big\langle \hat{\mathbf{E}}^-\hat{\mathbf{E}}^+ \big\rangle - \big(\big\langle \hat{\mathbf{E}}^+ \big\rangle - \big\langle \hat{\mathbf{E}}^- \big\rangle\big)^2 < 0\,. \quad (38)$$

We now recall that $\hat{\mathbf{E}}^+ \sim \hat{\sigma}^-$ and $\hat{\mathbf{E}}^- \sim \hat{\sigma}^+$ and also use expressions for $\langle \hat{\sigma}^+\hat{\sigma}^- \rangle$, $\langle \hat{\sigma}^+ \rangle$, and $\langle \hat{\sigma}^- \rangle$ (where σ^+ and σ^- are the respective atomic raising and lowering operators), which in a stationary state are [135, 162, 163]

$$\langle \hat{\sigma}^+\hat{\sigma}^- \rangle = \frac{(1/4)\Omega^2(1 + \Delta\omega_\mathrm{L}/\beta)}{(1/2)\Omega^2(1 + \Delta\omega_\mathrm{L}/\beta) + (\beta + \Delta\omega_\mathrm{L})^2 + \beta^2 D^2}\,,$$

$$\langle \hat{\sigma}^+ \rangle = \frac{(1/2)(\Omega/\beta)\big[\mathrm{i}(1 + \Delta\omega_\mathrm{L}/\beta) - D\big]}{(1/2)(\Omega^2/\beta^2)(1 + \Delta\omega_\mathrm{L}/\beta) + (1 + \Delta\omega_\mathrm{L}/\beta)^2 + D^2}\,,$$

$$\langle \hat{\sigma}^- \rangle = \big(\langle \hat{\sigma}^+ \rangle\big)^*.$$

We then obtain

$$\big\langle : (\Delta\hat{\mathbf{E}}_1)^2 : \big\rangle = \frac{Z^4(1 + \Delta\omega_\mathrm{L}/\beta)^2 + Z^2(1 + \Delta\omega_\mathrm{L}/\beta)^3 + Z^2D^2(1 + \Delta\omega_\mathrm{L}/\beta) - 2Z^2D^2}{\big(Z^2(1 + \Delta\omega_\mathrm{L}/\beta) + (1 + \Delta\omega_\mathrm{L}/\beta)^2 + D^2\big)^2}\,, \quad (39)$$

$$\big\langle : (\Delta\hat{\mathbf{E}}_2)^2 : \big\rangle = \frac{Z^4(1 + \Delta\omega_\mathrm{L}/\beta)^2 + Z^2(1 + \Delta\omega_\mathrm{L}/\beta)^3 + Z^2D^2(1 + \Delta\omega_\mathrm{L}/\beta) - 2Z^2(1 + \Delta\omega_\mathrm{L}/\beta)^2}{\big(Z^2(1 + \Delta\omega_\mathrm{L}/\beta) + (1 + \Delta\omega_\mathrm{L}/\beta)^2 + D^2\big)^2}\,, \quad (40)$$

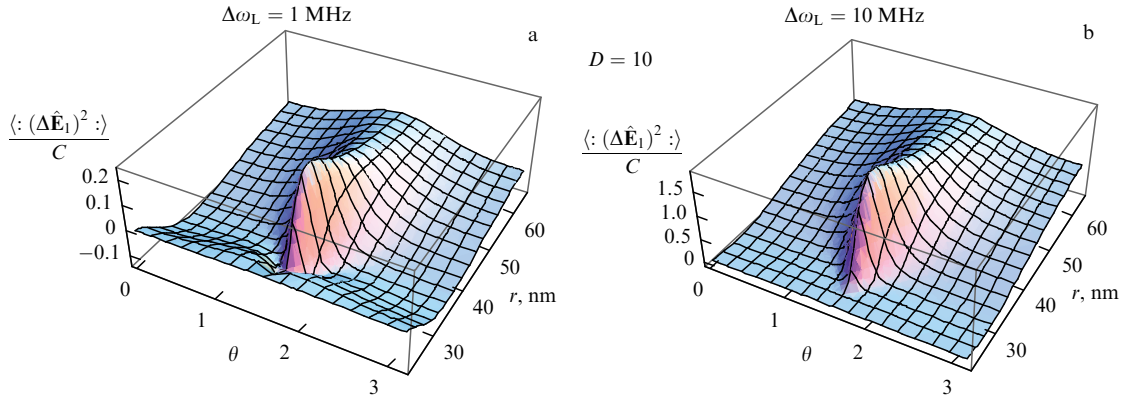

Figure 16. (Color online.) Dependence of the quantity $\langle : (\Delta\hat{\mathbf{E}}_1)^2 : \rangle$ normalized to C on the QE position at $D = 10$ for (a) $\Delta\omega_L = 1$ MHz and (b) $\Delta\omega_L = 10$ MHz in the presence of a spherical NP.

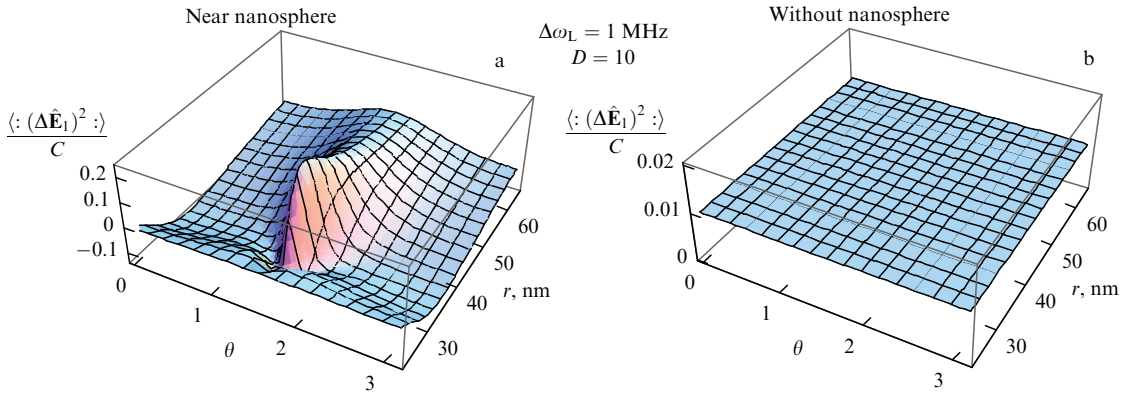

Figure 17. (Color online.) Dependence of the quantity $\langle : (\Delta\hat{\mathbf{E}}_1)^2 : \rangle$ normalized to C on the QE position at $D = 10$ (a) in the presence and (b) in the absence of an NP.

where $Z = \sqrt{2}\Omega/\gamma$. The squeezing conditions for $\hat{\mathbf{E}}_1$ and $\hat{\mathbf{E}}_2$ therefore become

$$Z^2\left(1+\frac{\Delta\omega_L}{\beta}\right)^2+\left(1+\frac{\Delta\omega_L}{\beta}\right)^3+D^2\left(1+\frac{\Delta\omega_L}{\beta}\right)-2D^2<0\,, \tag{41}$$

$$Z^2\left(1+\frac{\Delta\omega_L}{\beta}\right)+\left(1+\frac{\Delta\omega_L}{\beta}\right)^2+D^2-2\left(1+\frac{\Delta\omega_L}{\beta}\right)<0\,. \tag{42}$$

It is easy to show that inequalities (41) and (42) are incompatible.

In accordance with (41), the fluorescence radiation for $\hat{\mathbf{E}}_1$ is not squeezed if the exciting field is a totally resonance one, i.e., $D = 0$. But assuming $D = 0$, we have

$$Z^2+\left(1+\frac{\Delta\omega_L}{\beta}\right)<0$$

for $\hat{\mathbf{E}}_1$. This inequality is false, because all terms on the left-hand side are non-negative. For $\hat{\mathbf{E}}_2$, we find

$$Z^2+\frac{\Delta\omega_L}{\beta}<1\,,$$

whence it follows that $\Omega < \gamma$, i.e., the damping (spontaneous relaxation rate) is too high, and in this case the fluorescence spectrum contains only one central peak corresponding to an elastically scattered photon.

In [165], the squeezing of fluorescence radiation was discussed, but the linewidth of the exciting field was not taken into account. Results (41) and (42) obtained for $\Delta\omega_L \neq 0$ are in complete agreement with the results in [165] obtained at $\Delta\omega_L = 0$.

Figure 16 shows how $\langle : (\Delta\hat{\mathbf{E}}_1)^2 : \rangle$ normalized to C depends on the QE position near the nanosphere at $D = 10$ for different values of $\Delta\omega_L$ in the presence of a nanosphere. It can be seen that, as the laser linewidth increases, the radiation squeezing effect for the $\hat{\mathbf{E}}_1$ field component disappears. This directly follows from (41).

Figure 17 shows $\langle : (\Delta\hat{\mathbf{E}}_1)^2 : \rangle$ normalized to C for a QE in the presence and absence of a nanosphere for the detuning $D = 10$. It can be seen that, in the absence of the nanosphere at fixed parameters of the incident radiation, the fluorescence radiation is not squeezed. Due to the presence of a nanosphere, squeezing occurs near its surface. It can be seen from the results in (39) and (40) that the squeezing has a complicated dependence on the Rabi frequency Ω and on the spontaneous relaxation rate γ, which in turn depend on the QE position relative to the spherical NP.

There are also papers dealing with various quantum effects in QE + NP array systems. In particular, the effects of quantum coherence and interference in the QE near NPs were studied in [166], where the formation of dark states, optical pumping, coherent Raman scattering, and STIRAP (STImulated Raman Adiabatic Passage) in the presence of metallic NPs were demonstrated. It was shown that dark

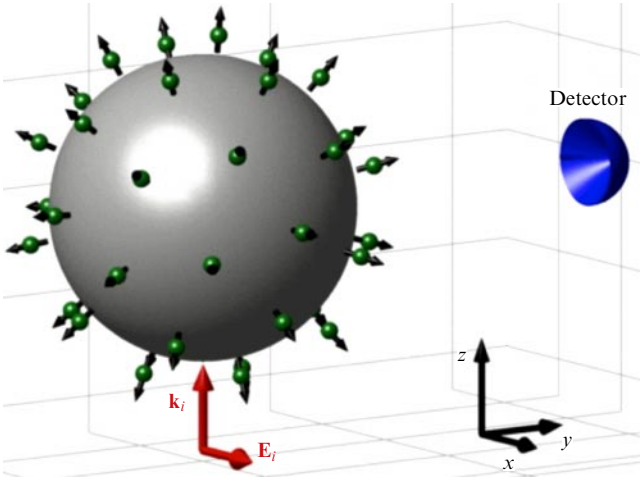

Figure 18. (Color online.) Scheme of the system under study: a metallic NP is surrounded by a set of QEs uniformly distributed in a spherical shell with a radial orientation of dipoles.

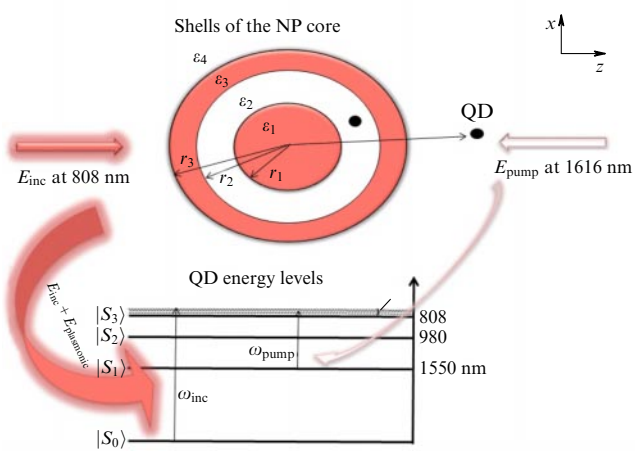

Figure 19. (Color online.) Scheme of coupling of a QD and NP with a Russian-doll structure to two colliding beams of laser radiation at frequencies of 808 and 1616 nm.

states are formed but have a more complex structure in the presence of NPs, and optical pumping and STIRAP cannot be used near NPs. The STIRAP method should be used with caution, because it can fail or at least acquire new functions in the presence of NPs.

In [167], a system consisting of metallic NPs and a set of QEs was considered (Fig. 18). In the case of a weak QE–NP coupling, the well-known phenomenon of fluorescence quenching occurs; in this regime, electromagnetic modes are regarded as a quasicontinuum. It was shown that the concept of quenching breaks down for a strong coupling between the QE and the NP electromagnetic modes. In this limit, the higher multipole modes can no longer be regarded as a quasicontinuum, and the pseudomode description becomes more appropriate. Using numerical and analytic modeling, the authors of [167] demonstrated that, in the case of weak coupling, the quenching pattern experiences essential changes under the transition to the strong coupling regime. In the weak coupling limit, the nonradiative NP electromagnetic modes act as an effective heat bath for the QE radiation, but under the transition to the strong coupling regime they become a pseudomode capable of reversibly exchanging energy with the QE. Energy transfer occurs between each emitter and the localized pseudomode and is therefore not a cooperative effect. But as the number of QEs increases, the collective strong coupling of many QEs to the NP radiative dipole mode increases even at very short distances.

An obvious development is to consider increasingly complex nanostructures. For example, in [168], the interaction between a QD and a core–double-shell NP (Fig. 19) was studied theoretically in the framework of an entirely quantum approach. The possibility of controlling spontaneous emission of a QD located near such particles and inside them (in shells) was considered. It was shown that NPs of the core–double-shell type, in contrast to simple NPs without shells, ensure the NP–QD switching of absorption saturation. This effect is especially pronounced when QDs are placed inside the shell. Such systems are of interest for the creation of quantum plasmonic sensors.

Also of interest are studies of NPs made of special materials. For example, in [169], the optical properties of an NP dimer based on a topological insulator and a QE interacting in a strong coupling regime were studied theoretically. Topologically protected (surface) states affect the optical properties of NPs based on a topological insulator (NTI), demonstrating that — similarly to a plasmon in a metal NP — a single electron in such a state creates a surface charge density under the action of light. In addition, such an electron can act as a protecting layer, effectively suppressing absorption inside the NP, and can couple phonons and light, inducing a previously undetectable topological polariton mode (TPM) of the NP. The authors of [169] theoretically (by calculating the system spectrum) studied the behavior of this mode in the case where the NTI is strongly coupled to a single QE. It was shown, in particular, that the TPM is strongly coupled to the QE resonance, inducing a hybrid mode, whose output signal, together with its spectral position, can be tuned by controlling the NTI size (Fig. 20), i.e., the distance between the NP and the QE.

The coherent interaction between a QE and photon modes in resonators underlies many current strategies aimed at creating and controlling quantum photon states. A plasmonic nanoresonator provides a successful solution for reducing the effective mode volumes to the nanometer scale, but spatial control of the coupling to a single molecular QE at the atomic level is challenging. The authors of [170] experimentally demonstrated subnanometer spatial control over the coherent bond between an individual molecule and a plasmon nanoresonator located in close proximity to each other by tracking the evolution of Fano line shapes and photon Lamb shifts in the spectra of electron-induced tunneling luminescence. The evolution of the Fano dips allows determining the effective interaction distance, which, based on experimental data, is 1 nm. Moreover, the binding strength reaches a value of about 15 meV, and giant self-coupling causes a photon Lamb shift up to ~ 3 meV. These results open up new possibilities for controlling quantum interference and the field–matter interaction at the nanoscale.

4.5 Generation of entangled quantum states

For applications that involve quantum entangled states, it is desirable that such states, once created, exist for a sufficiently long time [171–173]. The results of many studies, however, show that dissipative processes in the system and the decoherence associated with them are a serious obstruction to the preservation of entanglement. Nevertheless, this

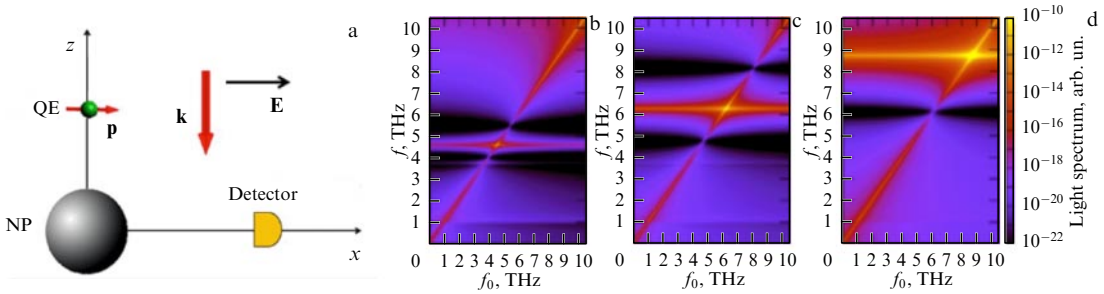

Figure 20. (Color online.) (a) Spectrum observation setup. NTI dimer (Bi_2Se_3) + QE system is illuminated by a normally incident field. Detector is placed at a very long distance so as to capture only far-field light components. (b–d) Spectra of the hybrid system under study for NTI with a radius of (b) 30 nm, (c) 20 nm, and (d) 10 nm. Coupling between the TPM and the QE resonance is enhanced and shifts toward higher frequencies as the NTI size decreases. Output coupling signal (middle of the avoided intersection region) and its spectral position can be tuned by simply controlling the NP size (system is assumed to be in the air).

intuitive statement turns out to be erroneous when it comes to generating entanglement by binding qubits to a common dissipative medium. Such schemes are extremely attractive from a practical standpoint, because they allow achieving entanglement regardless of the initial state of the system and, as has been shown, are quite robust with respect to changes in control parameters. Metallic NPs can serve as such dissipative media.

Initially, metal nanowires were considered as such nanostructures. Surface plasmon polaritons that can be excited in them propagate along the nanowires. In such a geometry, the quantum states of qubits represented by QDs, atoms, or even molecules can be entangled if they are brought close to the nanowire. For identical qubits, the maximum degree of entanglement can be obtained by choosing an appropriate relative strength of their coupling to the nanowire. In such a scheme, multiparticle entanglement between qubits and plasmons is achieved, followed by the measurement of the number of plasmonic excitations at the ends of the nanowire. Only when the plasmons are not detected can it be concluded that the qubits were maximally entangled with each other.

A proposal to circumvent this probabilistic nature of obtaining entangled states and create a high degree of entanglement in deterministic circuits involved placing the qubits asymmetrically with respect to the nanowire. At certain values of the coupling strength, the maximum degree of entanglement can be achieved regardless of the state of the plasmon field [174, 175]. However, the large losses associated with the propagation of surface plasmons do not allow entanglement to be maintained for long periods of time.

The idea of using loss channels to transfer qubits to a subradiative dissipation-resistant state was investigated in [176]. The described scenario allows achieving stationary entanglement. This requires the system to be initially brought into a predetermined state; the resulting entanglement remains well below the maximum possible.

Recently, a loss-tolerant entanglement generation scheme with a waveguide consisting of a chain of metallic NPs was proposed [177], while nanoscale optical gratings were proposed to control the interaction of distant ultracold atoms via their coupling to collective plasmonic modes [178].

Still, none of the schemes described above can ensure the maximum stationary entanglement of a pair of qubits in a deterministic way. To achieve it, the use of strongly dissipative systems has been proposed.

Along with studies on the propagation of surface plasmon polaritons in metal waveguides, an isolated metal nanoantenna was treated as a dissipative structure in some studies. In [179], a scheme is proposed for creating the maximum-entangled two-qubit state using a dissipatively controlled process. For this, the quantum qubit states coupled via a plasmonic nanoantenna are entangled (Fig. 21a). When a weak spectral asymmetry is imposed on the properties of the qubits, the probability of obtaining the maximum-entangled subradiative state approaches unity. This is despite the high losses associated with the plasmonic nanoantenna, which are generally considered detrimental. The authors of [179] showed that the entanglement scheme is quite stable to changes in QD transition frequencies and deviations in their prescribed position relative to the nanoantenna, and the maximum entanglement can be obtained using a symmetric coupling constant.

A similar system was studied in [180], where two identical QEs were located near a spherical metal NP. The dipole plasmon resonance frequency coincides with the QE radiative transition frequency (Fig. 21b). A scheme has been proposed where two QEs are resonantly coupled to an NP dipole plasmon resonance, with only one QE excited initially. In this scheme, a stable coherent superposition state can be formed much faster than the spontaneous emission of an isolated QE can occur. In this superposition state, the nonzero QE dipole moments are out of phase with each other, and hence the total electric field acting on the NP vanishes, thus eliminating energy dissipation (i.e., field absorption in the NP) and significantly increasing the lifetime of the entangled state. It was shown that the degree of stationary entanglement depends only on the ratio of distances between the QE and the NP, reaching the maximum value of 0.65 when the distance between the NP and the initially excited QE is 20% greater than the distance from another QE to the NP (Fig. 21c).

A feature of the process under consideration is that, despite the nonzero dissipation in the QE–NP–QE system (due to the absorption of NP radiation), the stationary entanglement remains constant for a time much longer than the characteristic time of the system, until a much slower process of spontaneous emission begins.

In [181], a similar system consisting of two QD qubits coupled to a common evanescent mode of surface plasmons was considered, but — in contrast to the QDs in the scheme proposed in [180] — each QD was also coupled to a separate photon resonator mode (Fig. 21d). The QDs and plasmons were excited by a 20-fs laser pulse. The QD entanglement defined as the Wooters coincidence degree can be detected by

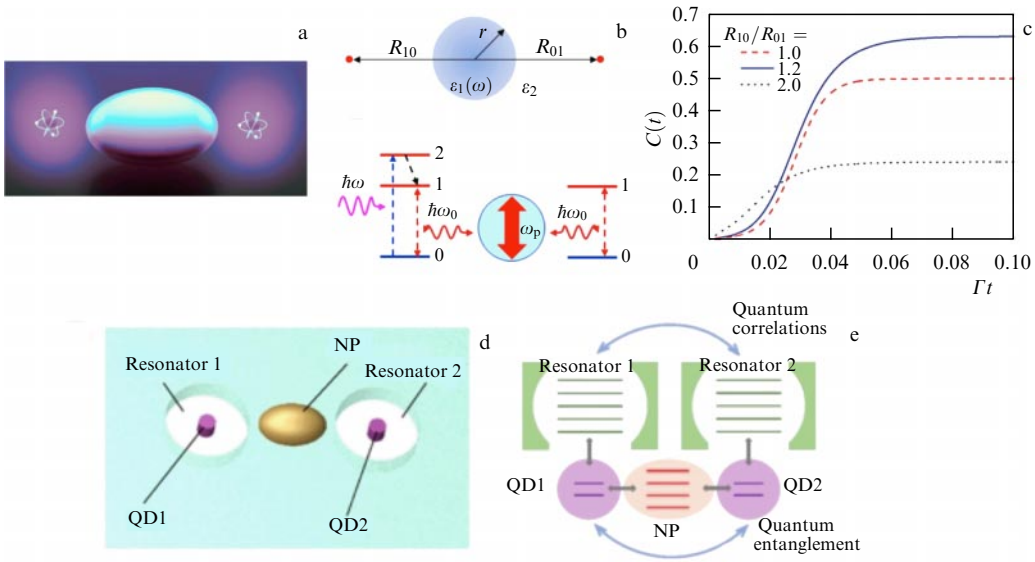

Figure 21. (Color online.) (a) Scheme of the system studied in [179]: two qubits (atoms, molecules, or QDs) located near an optical nanoantenna in the form of an ellipsoid (only the electric dipole moment of the nanoantenna is taken into account). (b) Scheme of the system studied in [180]. (c) Coincidence rate as a function of the normalized time for various QE–NP distances. (d) Scheme of the system studied in [181], and (e) its graphical representation: two-level QDs are coupled to plasmon modes and photon resonator modes.

measuring the correlation function $g^{(2)}(\tau)$ of a resonator photon and can be preserved in high-Q optical resonators.

A similar approach, with a second-order time correlation function used as an indication of the presence of entanglement between a pair of qubits associated with a common plasmonic nanostructure, was considered analytically and numerically in [182].

Further progress is associated with an increase in the number of QEs and NPs in the system. In [183], two, three, and four QDs were considered near a plasmonic nanosystem consisting of metallic NPs (Fig. 22a); the extension to an arbitrary number of QDs was studied in [184]. A system was proposed in which the control of the coupling of entangled QDs to a dissipative medium (plasmonic system) is determined by the nanoscale geometry of the system, and the only requirement for external parameters is an ultrafast laser pulse (single or repetitive).

Unlike schemes based on plasmonic waveguides, which can entangle spatially separated QDs but are limited to two QDs, the proposed scheme allows creating and maintaining entanglement between all pairs of QDs when two, three, etc. closely located QDs are coupled to a common plasmonic nanostructure. In that scheme, moreover, the entire system is initially in the ground state and is excited by a common laser pulse or a series of pulses.

In all cases, a high degree of coincidence is achieved only for a short period of time after the excitation of the system by a laser pulse, before the population of the entangled state decays. However, entanglement can be restored after applying a repeated train of pulses, as shown for the system of three QDs in Fig. 22b. Changing the strength of the coupling between each QD and the plasmonic nanostructure allows generating an excited state that spontaneously develops toward an entangled state due to the dissipation of plasmons. Entanglement is achieved without the need to address individual QDs.

The dynamics of two qubits located near a plasmonic nanostructure in the form of a two-dimensional lattice of metal-coated dielectric NPs was also considered in [186]. Each of the qubits locally, independently of the other, interacts with the plasmonic nanostructure. Two cases were considered in [186]: two identical two-level systems and two identical three-level V-type systems in which one two-level transition plays the role of a qubit and the other level acts as an auxiliary one. A two-dimensional lattice of metal-coated dielectric NPs was taken as a plasmonic nanostructure. The presence of this nanostructure can lead to strongly suppressed spontaneous emission rates of individual quantum systems, as well as to highly anisotropic spontaneous decay rates for orthogonal dipole matrix elements due to the anisotropic Purcell effect, which leads to quantum interference in spontaneous emission. Both effects can be used to dramatically change the entanglement dynamics of a system.

Most of the work on dissipation-controlled entanglement is limited to two qubits, and multiqubit entanglement is studied very little due to the computational complexity. In [185], a scheme with a large number of QDs located in the same plane around a spherical plasmonic NP was considered. Because the number of qubits is large, the number of combinations of control parameters increases exponentially. In modeling multiqubit entanglement, control parameters are usually chosen to be symmetric for different qubits, but previous studies show that the asymmetry of the control parameters, especially asymmetric detuning, plays an important role in two-qubit systems; therefore, asymmetric detuning also plays an important role in multiqubit entanglement.

The authors proposed an efficient model of a multiqubit system that allows reducing the computational complexity of the problem. A scalable plasmon system consisting of a multiqubit and a dissipative NP was designed to generate multiqubit dissipation-controlled entanglement (Fig. 22c). Numerical simulation of the plasmon system using the effective model shows that stationary entanglement caused by nonzero asymmetric detuning is much larger than the one at resonance. In addition, the number of qubit pairs with antisymmetric detuning is important for enhancing entangle-

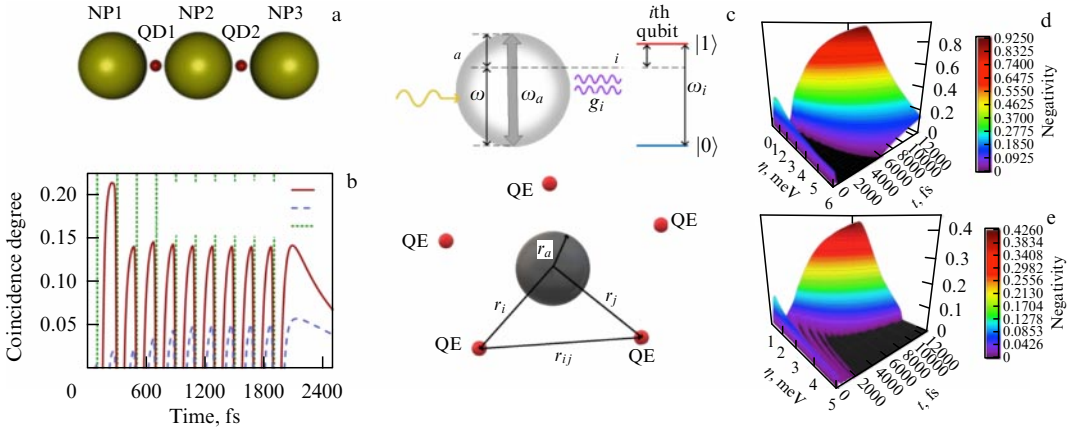

Figure 22. (Color online.) (a) Diagram of the system studied in [183]. (b) Degree of coincidence as a function of time for a system of three QDs and a plasmonic nanostructure. (c) System studied in [185], consisting of several qubits near a nanosphere with parameters shown in the figure. Qubits, whose number can be varied, are located on a fixed plane passing through the center of the nanosphere. Negativity as a function of time and the control field for (d) a two-qubit system when the control field is zero and (e) a three-qubit system when the control field is large (> 5 MeV). Initial states are set equal to $|100\rangle$; control field is in resonance with the plasmon mode.

ment, and the maximum entanglement is obtained by an appropriate combination of control parameters. Analytic and numerical calculations have shown that the abrupt disappearance of entanglement and its subsequent revival occur when the control field is sufficiently high (> 5 MeV) (Fig. 22e); negativity is chosen as the entanglement criterion [187].

We note, importantly, that direct experimental observation of entanglement in such systems is an extremely difficult task at present; research is therefore mostly concentrated in the area of theory.

5. Conclusion

We have discussed the QE quantum optics effects in the near field of an NP. The mechanisms for modifying the radiative and nonradiative decay rates in the simplest two-level QE model near a plasmonic NP are described, and the near-field strength and polarization distribution around the NP is analyzed. This distribution has a complex structure, which essentially depends on the polarization of the external radiation field and the parameters of NP plasmon resonances. Quantum optics effects in the (NP + QE) + external laser field system are also analyzed, including the modification of the resonance QE fluorescence spectrum in the near field, bunching/antibunching and quantum statistics of photons in the spectrum, the formation of squeezed states of light, and quantum entangled states in such systems.

Research in these areas has been thriving from year to year, but, due to the complexity of experiments, is mostly theoretical. However, the development of experimental techniques in nanophotonics is not standing still, and in the coming years these studies will hopefully be increasingly drifting toward experiment.

We schematically describe possible experiments on studying the near-field properties of a QE + NP system by detecting and subsequently analyzing QE resonance fluorescence spectra in the far field (Fig. 23). In the first of these (Fig. 23, left), the near field around the NP can be measured using a QE (fluorescent molecules or a QD) embedded in a polymer film deposited on a dielectric substrate. The NP is attached to the tip of a microscope, which can be placed in close proximity to one of the QEs. The QE + NP system is excited by incident laser radiation with the required polarization [72, 74]. By measuring the resonance fluorescence spectrum of the QE in the far zone, we can then obtain information about both the field strength and polarization of the near field at the spatial point where the QE is located [131].

An alternative experiment can be carried out with a dielectric NP located above or on a dielectric substrate, as is done in the experiment in [42, 43]: the QE (for example, a nanodiamond with an NV center) can be embedded into a probe that can be placed in the vicinity of the NP with high precision [46]. The resonance fluorescence spectrum of this QE, measured in the far field, then gives detailed information about the near-field strength and polarization at the point where the QE is located (Fig. 23, right).

The strategy of 3D polarization mapping, which is different from the ideas of these experiments, is as follows. An NP is placed in a viscous liquid containing fluorescent molecules (QEs), which slowly descend into the liquid under the action of gravity (or rise gently under the action of uniform heating). The QEs moving around the NP are recorded in one of the polarization-sensitive schemes using single-molecule nanoscopy, which allows accurately determining the spatial orientation of the molecule [47].

We also single out those areas that are currently relevant and will of course see active development in the near future. Among them are studies related to the interaction of structured light with chiral nanostructures [188–193] and dielectric NPs with a high refractive index [194–197]. We also note experimental studies of the interference effects arising from the interaction of NPs and QEs. One of them is the so-called cloaking effect [198]. It is well known from ordinary optics that macroscopic objects cast a shadow when illuminated by a beam of light, and the shadow becomes darker as the medium is made optically thicker. This scenario remains valid at the nanoscale, when the size of the object is smaller than the wavelength of light. For example, a gold NP less than 100 nm in diameter can quench more than half the power of a laser beam if placed in the focus. According to the Beer–Lambert law, this shadow becomes exponentially darker as more particles are added. In practice, a metallic NP can be made practically invisible when illuminated with

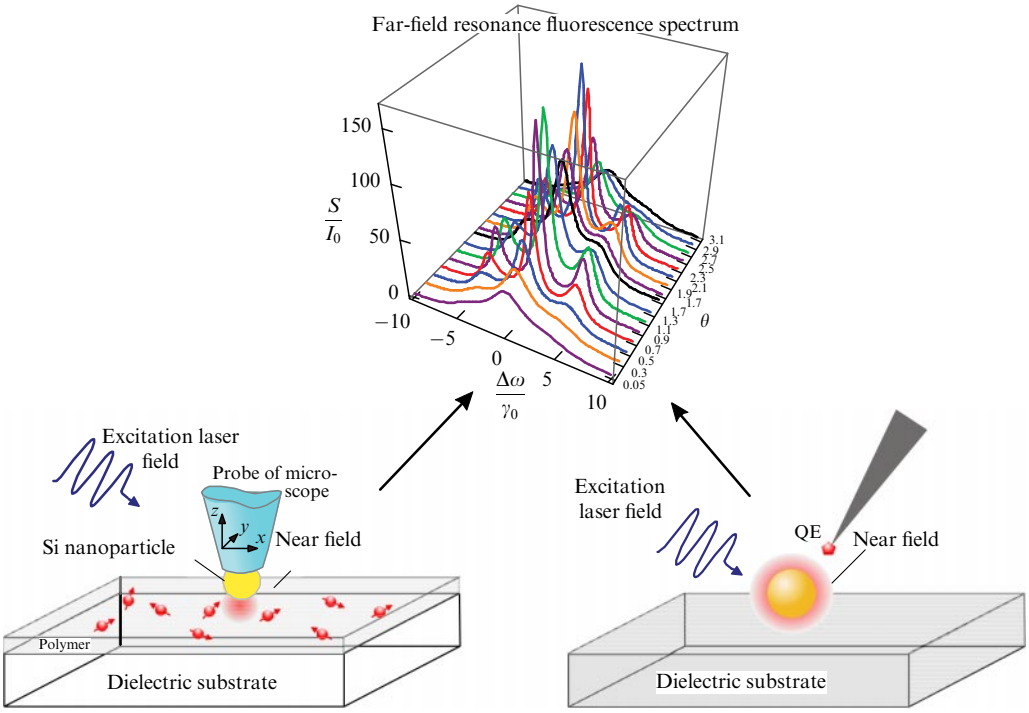

Figure 23. (Color online.) Diagram of two possible experiments to measure the near-field parameters (field strength and polarization) of an NP by detecting the far-field resonance fluorescence spectrum of a QE interacting with the NP.

light when a QE in resonance with the incident light frequency is placed properly in the path of the light beam.

The authors acknowledge financial support from the Russian Foundation for Basic Research, project 19-12-50258, and thank V V Klimov, B S Lukyanchuk, G Leuchs, P Banzer, E D Chubchev, and V M Pastukhov for the numerous discussions of the results of this work.

References

1. Tame M S et al. *Nat. Phys.* **9** 329 (2013)
2. Diedrich F, Walther H *Phys. Rev. Lett.* **58** 203 (1987)
3. Short R, Mandel L *Phys. Rev. Lett.* **51** 384 (1983)
4. Kimble H J, Dagenais M, Mandel L *Phys. Rev. Lett.* **39** 691 (1977)
5. Gaponenko S V *Introduction to Nanophotonics* (New York: Cambridge Univ. Press, 2010)
6. Liu Z et al. *Metamaterials* **2** 45 (2008)
7. Hatab N A et al. *Nano Lett.* **10** 4952 (2010)
8. Nien L-W et al. *J. Phys. Chem. C* **117** 25004 (2013)
9. Purcell E M, Torrey H C, Pound R V *Phys. Rev.* **69** 37 (1946)
10. Krasnok A E et al. *Nanoscale* **6** 7354 (2014)
11. Alù A, Engheta N *Nat. Photon.* **2** 307 (2008)
12. Engheta N *Science* **317** 1698 (2007)
13. Guo R et al. *Nano Lett.* **15** 3324 (2015)
14. Koenderink A F *Nano Lett.* **9** 4228 (2009)
15. Nayak P K et al. *Nat. Rev. Mater.* **4** 269 (2019)
16. Vladimirova Yu V et al. *Moscow Univ. Phys. Bull.* **73** 678 (2018); *Vestn. Moscow Univ. Ser. 3 Fiz. Astron.* (6) 99 (2018)
17. Dennler G et al. *J. Mat. Res.* **20** 3224 (2005)
18. Wang G et al. *ACS Sustainable Chem. Eng.* **2** 1331 (2014)
19. Cheng P, Li Y, Zhan X *Energy Environment. Sci.* **7** 2005 (2014)
20. West J L, Halas N J *Annu. Rev. Biomed. Eng.* **5** 285 (2003)
21. Tam F et al. *Nano Lett.* **7** 496 (2007)
22. Hirsch L R et al. *Proc. Natl. Acad. Sci. USA* **100** 13549 (2003)
23. Loo C et al. *Nano Lett.* **5** 709 (2005)
24. O'Neal D P et al. *Cancer Lett.* **209** 171 (2004)
25. Kim K et al. *Small* **8** 892 (2012)
26. Wertz E et al. *Nano Lett.* **15** 2662 (2015)
27. Krasnok A E et al. *Phys. Usp.* **56** 539 (2013); *Usp. Fiz. Nauk* **183** 561 (2013)
28. Klimov V V *Phys. Usp.* **51** 839 (2008); *Usp. Fiz. Nauk* **178** 875 (2008)
29. Lepeshov S I et al. *Phys. Usp.* **61** 1035 (2018); *Usp. Fiz. Nauk* **188** 1137 (2018)
30. Novotny L, van Hulst N *Nat. Photon.* **5** 83 (2011)
31. Hernandez F E, in *Reviews in Plasmonics 2010* (Ed. C D Geddes) (New York: Springer, 2012) p. 185
32. Novotny L A, Hecht B *Principles of Nano-Optics* (New York: Cambridge Univ. Press, 2012)
33. Maier S A *Plasmonics: Fundamentals and Applications* (New York: Springer, 2007)
34. Klimov V V *Nanoplazmonika* (Moscow: Fizmatlit, 2009)
35. Klimov V V *Nanoplasmonics* (Singapore: Pan Sanford Publ., 2014)
36. Boltasseva A, Atwater H A *Science* **331** 290 (2011)
37. Boriskina S V et al. *Adv. Opt. Photon.* **9** 775 (2017)
38. Mohamed M B et al. *Chem. Phys. Lett.* **317** 517 (2000)
39. Baffou G, Quidant R *Laser Photon. Rev.* **7** 171 (2013)
40. Baranov D G et al. *Optica* **4** 814 (2017)
41. Mie G *Ann. Physik* **330** 377 (1908)
42. Feng T et al. *ACS Photon.* **5** 678 (2018)
43. Zambrana-Puyalto X, Bonod N *Phys. Rev. B* **91** 195422 (2015)
44. Mandel L, Wolf E *Optical Coherence and Quantum Optics* (Cambridge: Cambridge Univ. Press, 1995); Translated into Russian: *Opticheskaya Kogerentnost' i Kvantovaya Optika* (Moscow: Nauka, 2000)
45. Bohren C F, Huffman D R, in *Absorption and Scattering of Light by Small Particles* (Eds C F Bohren, D R Huffman) (Weinheim: Wiley-VCH, 1998) p. 544
46. Klimov V V, Ducloy M, Letokhov V S *J. Mod. Opt.* **43** 549 (1996)
47. Li L-W, Kang X-K, Leong M-S *Spheroidal Wave Functions in Electromagnetic Theory* (New York: John Wiley and Sons, 2002)
48. Falloon P E "Theory and computation of spheroidal harmonics with general arguments", Master Thesis (Pert: The Univ. of Western Australia, 2001)
49. Voitovich N N, Katsenelenbaum B Z, Sivov A N *Obobshchennyi Metod Sobstvennykh Kolebanii v Teorii Difraktsii* (Generalized Method of Eigenoscillations in Diffraction Theory) (Moscow: Nauka, 1977)

50. Voitovich N N, Katsenelenbaum B Z, Sivov A N *Sov. Phys. Usp.* **19** 337 (1976); *Usp. Fiz. Nauk* **118** 709 (1976)
51. Chubchev E D, Vladimirova Yu V, Zadkov V N *Opt. Express* **22** 20432 (2014)
52. Chubchev E D, Vladimirova Yu V, Zadkov V N *Laser Phys. Lett.* **12** 015302 (2015)
53. Setälä T et al. *Phys. Rev. E* **66** 016615 (2002)
54. Grigoriev K S et al. *Phys. Rev. A* **98** 063805 (2018)
55. Kumar G V P *J. Nanophoton.* **6** 064503 (2012)
56. Vladimirova Yu V, Pavlov A A, Zadkov V N *Moscow Univ. Phys. Bull.* **72** 544 (2017); *Vestn. Moscow Univ. Ser. 3. Fiz. Astron.* (6) 49 (2017)
57. Reshetov S A et al. *EPJ Web Conf.* **132** 03006 (2017)
58. Vladimirova Yu V et al. *Phys. Rev. A* **100** 023847 (2019)
59. Kuznetsov N Yu et al. *Opt. Express* **28** 27293 (2020)
60. Alferov Zh I *Rev. Mod. Phys.* **73** 767 (2001)
61. Wu D et al. *Chem. Soc. Rev.* **46** 7105 (2017)
62. Stehr F et al. *Nat. Commun.* **10** 1268 (2019)
63. Ray S, Widom J R, Walter N G *Chem. Rev.* **118** 4120 (2018)
64. Ecker J R et al. *Neuron* **96** 542 (2017)
65. Andersen C M, Mortensen G *J. Agric. Food Chem.* **56** 720 (2008)
66. Fothergill S M, Joyce C, Xie F *Nanoscale* **10** 20914 (2018)
67. Koenderink A F *Opt. Lett.* **35** 4208 (2010)
68. Sauvan C et al. *Phys. Rev. Lett.* **110** 237401 (2013)
69. Bitton O, Gupta S N, Haran G *Nanophotonics* **8** 559 (2019)
70. Klimov V V, Letokhov V S, Ducloy M *Phys. Rev. A* **56** 2308 (1997)
71. Klimov V V, Letokhov V S *J. Exp. Theor. Phys.* **84** 24 (1997); *Zh. Eksp. Teor. Fiz.* **111** 44 (1997)
72. Klimov V V, Ducloy M, Letokhov V S *J. Mod. Opt.* **44** 1081 (1997)
73. Klimov V V, Ducloy M, Letokhov V S *Phys. Rev. A* **59** 2996 (1999)
74. Haroche S, in *Fundamental Systems in Quantum Optics*: *Les Houches, Session LIII* (Eds J Dalibard, J-M Raimond, J Zinn-Justin) (Amsterdam: North-Holland, 1992) p. 767
75. Klimov V V, Ducloy M *Phys. Rev. A* **69** 013812 (2004)
76. Klimov V V *Phys. Usp.* **46** 979 (2003); *Usp. Fiz. Nauk* **173** 1008 (2003)
77. Wylie J M, Sipe J E *Phys. Rev. A* **30** 1185 (1984)
78. Wylie J M, Sipe J E *Phys. Rev. A* **32** 2030 (1985)
79. Dung H T, Knöll L, Welsch D-G *Phys. Rev. A* **62** 05380 (2000)
80. Knoll L, Scheel S, Welsch D-G, quant-ph/0006121
81. Yeung M S, Gustafson T K *Phys. Rev. A* **54** 5227 (1996)
82. Drexhage K H *Ber. Bunsenges. Phys. Chem.* **20** 1176 (1966)
83. Goy P et al. *Phys. Rev. Lett.* **50** 1903 (1983)
84. Kleppner D *Phys. Rev. Lett.* **47** 233 (1981)
85. Andrew P, Barnes W L *Science* **290** 785 (2000)
86. Pohl D W, in *Near-Field Optics. Principles and Applications, Proceedings of the Second Asia-Pacific Workshop, Beijing, China, 20–23 October 1999* (Eds X Zhu, M Ohtsu) (Singapore: World Scientific, 2000) p. 9
87. Anger P, Bharadwaj P, Novotny L *Phys. Rev. Lett.* **96** 113002 (2006)
88. Kühn S et al. *Phys. Rev. Lett.* **97** 017402 (2006)
89. Girard C et al. *Chem. Phys. Lett.* **404** 44 (2005)
90. Koenderink A F *ACS Photon.* **4** 710 (2017)
91. Sullivan K G, Hall D G *J. Opt. Soc. Am. B* **14** 1149 (1997)
92. Amos R M, Barnes W L *Phys. Rev. B* **55** 7249 (1997)
93. Chance R R, Prock A, Silbey R, in *Advances in Chemical Physics* Vol. 37 (Eds I Prigogine, S A Rice) (New York: John Wiley, 1978) p. 1
94. Wu S-T, Eberlein C *Proc. R. Soc. Lond. A* **455** 2487 (1999)
95. Chew H *J. Chem. Phys.* **87** 1355 (1987)
96. Klimov V V, Ducloy M, Letokhov V S *J. Mod. Opt.* **43** 2251 (1996)
97. Katsenelenbaum B Z *Zh. Tekh. Fiz.* **19** 1182 (1949)
98. Nha H, Jhe W *Phys. Rev. A* **56** 2213 (1997)
99. Enderlein J *Chem. Phys. Lett.* **301** 430 (1999)
100. Żakowicz W, Janowicz M *Phys. Rev. A* **62** 013820 (2000)
101. Klimov V V, Ducloy M *Phys. Rev. A* **62** 043818 (2000)
102. Klimov V V, Ducloy M, Letokhov V S *Eur. Phys. J. D* **20** 133 (2002)
103. Klimov V V, Ducloy M, Letokhov V S *Chem. Phys. Lett.* **358** 192 (2002)
104. Klimov V V *JETP Lett.* **68** 641 (1998); *Pis'ma Zh. Eksp. Teor. Fiz.* **68** 610 (1998)
105. Klimov V V, Perventsev Ya A *Quantum Electron.* **29** 847 (1999); *Kvantovaya Elektron.* **29** 9 (1999)
106. Zijlstra P, Paulo P, Orrit M *Nat. Nanotechnol.* **7** 379 (2012)
107. Kinkhabwala A et al. *Nat. Photon.* **3** 654 (2009)
108. Punj D et al. *Nat. Nanotechnol.* **8** 512 (2013)
109. Karamlou A, Trusheim M E, Englund D *Opt. Express* **26** 3341 (2018)
110. Guzatov D V, Klimov V V, Pikhota M Yu *Laser Phys.* **20** 85 (2010)
111. Guzatov D V, Klimov V V *Chem. Phys. Lett.* **412** 341 (2005)
112. Guzatov D V, Klimov V V *New J. Phys.* **13** 053034 (2011)
113. Klimov V V, Guzatov D V *Appl. Phys. A* **89** 305 (2007)
114. Curto A G et al. *Science* **329** 930 (2010)
115. Aouani H et al. *Nano Lett.* **11** 2400 (2011)
116. Langguth L et al. *ACS Nano* **7** 8840 (2013)
117. Belacel C et al. *Nano Lett.* **13** 1516 (2013)
118. Mohtashami A et al. *ACS Photon.* **1** 1134 (2014)
119. Hoang T B, Akselrod G M, Mikkelsen M H *Nano Lett.* **16** 270 (2016)
120. Krasnok A E et al. *Opt. Express* **20** 20599 (2012)
121. Rolly B, Stout B, Bonod N *Opt. Express* **20** 20376 (2012)
122. Rusak E et al. *Appl. Phys. Lett.* **105** 221109 (2014)
123. Regmi R et al. *Nano Lett.* **16** 5143 (2016)
124. Bouchet D et al. *Phys. Rev. Appl.* **6** 064016 (2016)
125. Wang H et al. *ACS Nano* **9** 436 (2015)
126. Klimov V V, Guzatov D V *Phys. Rev. B* **75** 024303 (2007)
127. Klimov V V, Guzatov D V *Quantum Electron.* **37** 209 (2007); *Kvantovaya Elektron.* **37** 209 (2007)
128. Sun S et al. *J. Phys. Chem. C* **121** 12871 (2017)
129. Sun S et al. *J. Phys. Chem. C* **123** 21150 (2019)
130. Sun S et al. *J. Phys. Chem. C* **122** 14771 (2018)
131. Vladimirova Yu V et al. *Phys. Rev. A* **85** 053408 (2012)
132. Apanasevich P A *Opt. Spektrosk.* **14** 324 (1963)
133. Apanasevich P A *Opt. Spektrosk.* **16** 387 (1964)
134. Newstein M C *Phys. Rev.* **167** 89 (1968)
135. Mollow B R *Phys. Rev.* **188** 1969 (1969)
136. Walther H, in *Advances in Atomic, Molecular and Optical Physics* Vol. 51 (Ed. H H Stroke) (Amsterdam: Elsevier, 2005) p. 239
137. Kimble H J, Mandel L *Phys. Rev. A* **13** 2123 (1976)
138. Klimov V V, Letokhov V S, Ducloy M *Laser Phys.* **17** 912 (2007)
139. Andrianov E S et al. *JETP Lett.* **97** 452 (2013)è *Pis'ma Zh. Eksp. Teor. Fiz.* **97** 522 (2013)
140. Trügler A, Hohenester U *Phys. Rev. B* **77** 115403 (2008)
141. Carreño F et al. *Phys. Rev. A* **94** 013834 (2016)
142. Carreño F et al. *Phys. Rev. A* **95** 043825 (2017)
143. Sanchez-Munoz C, Gonzalez-Tudela A, Tejedor C *Phys. Rev. B* **85** 125301 (2012)
144. Sadeghi S M *Appl. Phys. Lett.* **101** 213102 (2012)
145. Ge R-C et al. *Phys. Rev. B* **87** 205425 (2013)
146. Sadeghi S M *Phys. Rev. A* **88** 013831 (2013)
147. Slowik K et al. *Phys. Rev. B* **88** 195414 (2013)
148. Theuerholz T S et al. *Phys. Rev. B* **87** 245313 (2013)
149. Fang W et al. *Phys. Rev. A* **93** 053831 (2016)
150. Astafiev O et al. *Science* **327** 840 (2010)
151. Pastukhov V V, Vladimirova Yu V, Zadkov V N *Phys. Rev. A* **90** 0638310 (2014)
152. Smirnov D F, Troshin A S *Sov. Phys. Usp.* **30** 851 (1987); *Usp. Fiz. Nauk* **153** 233 (1987)
153. Carmichael H J, Walls D F *J. Phys. B* **9** L43 (1976)
154. Cohen-Tannoudji C, in *Frontiers in Laser Spectroscopy, Les Houches, Session XXVII, 1975* (Eds R Balian, S Haroche, S Liberman) (Amsterdam: North-Holland, 1977) p. 1
155. Glauber R J *Phys. Rev.* **130** 2529 (1963)
156. Glauber R J *Phys. Rev.* **131** 2766 (1963)
157. Abramowitz M, Stegun I A (Eds) *Handbook of Mathematical Functions, with Formulas, Graphs, and Mathematical Tables* (New York: Dover Publ., 1965) Sec. 3.8.2
158. Carreño F et al. *Phys. Rev. A* **100** 023802 (2019)
159. Sáez-Blázquez R et al. *Phys. Rev. A* **98** 013839 (2018)
160. Bordo V G *Phys. Rev. A* **100** 063807 (2019)
161. Phillips C L et al. *Phys. Rev. Lett.* **125** 043603 (2020)
162. Kimble H J, Mandel L *Phys. Rev. A* **15** 689 (1977)
163. Walls D F *J. Phys. B* **13** 2001 (1980)
164. Mandel L *Phys. Rev. Lett.* **49** 136 (1982)
165. Walls D F, Zoller P *Phys. Rev. Lett.* **47** 709 (1981)
166. Dhayal S, Rostovtsev Yu V *Phys. Rev. A* **93** 043405 (2016)

167. Delga A et al. *Phys. Rev. Lett.* **112** 253601 (2014)
168. Ahmad S *Phys. Rev. A* **94** 043819 (2016)
169. Chatzidakis G D, Yannopapas V *Phys. Rev. B* **101** 165410 (2020)
170. Zhang Y et al. *Nat. Commun.* **8** 15225 (2017)
171. Reilly D J *npj Quantum Inf.* **1** 15011 (2015)
172. Pan J-W et al. *Rev. Mod. Phys.* **84** 777 (2012)
173. Bargatin I V, Grishanin B A, Zadkov V N *Phys. Usp.* **44** 597 (2001); *Usp. Fiz. Nauk* **171** 625 (2001)
174. Chen G-Y, Li C-M, Chen Y-N *Opt. Lett.* **37** 1337 (2012)
175. Jin X R, Gao J *Opt. Lett.* **38** 2110 (2013)
176. Martín-Cano D et al. *Phys. Rev. B* **84** 235306 (2011)
177. Lee C et al. *New J. Phys.* **15** 083017 (2013)
178. Gullans M et al. *Phys. Rev. Lett.* **109** 235309 (2012)
179. Hou J et al. *Phys. Rev. B* **89** 235413 (2014)
180. Nerkararyan K V, Bozhevolnyi S I *Phys. Rev. B* **92** 045410 (2015)
181. Otten M, Gray S K, Kolmakov G V *Phys. Rev. A* **99** 032339 (2019)
182. Dumitrescu E, Lawrie B *Phys. Rev. A* **96** 053826 (2017)
183. Otten M et al. *Phys. Rev. B* **92** 125432 (2015)
184. Otten M et al. *Phys. Rev. A* **94** 022312 (2016)
185. Tang W et al. *Phys. Rev. B* **100** 165415 (2019)
186. Iliopoulos N et al. *Phys. Rev. B* **96** 075405 (2017)
187. Vidal G, Werner R F *Phys. Rev. A* **65** 032314 (2002)
188. Lodahl P et al. *Nature* **541** 473 (2017)
189. De Leon I et al. *Sci. Rep.* **5** 13034 (2015)
190. Guzatov D V, Klimov V V *Phys. Rev. A* **98** 013823 (2018)
191. Guzatov D V, Klimov V V *New J. Phys.* **14** 123009 (2012)
192. Klimov V V, Guzatov D V *Phys. Usp.* **55** 1054 (2012); *Usp. Fiz. Nauk* **182** 1130 (2012)
193. Klimov V V, Guzatov D V, in *Singular and Chiral Nanoplasmonics* (Eds S V Boriskina, N I Zheludev) (Singapore: Pan Sanford Publ., 2014) p. 121
194. Woźniak P, Banzer P, Leuchs G *Laser Photon. Rev.* **9** 231 (2015)
195. Zambrana-Puyalto X et al. *ACS Photon.* **5** 2936 (2018)
196. Bauer T et al. *Appl. Phys. Lett.* **106** 091108 (2015)
197. Klimov V *Opt. Lett.* **45** 4300 (2020)
198. Zirkelbach J et al. *Phys. Rev. Lett.* **125** 103603 (2020)